Modelling snowpack dynamics and surface energy budget in boreal and subarctic peatlands and forests

Jari-Pekka Nousu[1,2,3], Matthieu Lafaysse[2], Giulia Mazzotti[2], Pertti Ala-aho[1], Hannu Marttila[1], Bertrand Cluzet[4], Mika Aurela[5], Annalea Lohila[5,6], Pasi Kolari[6], Aaron Boone[7], Mathieu Fructus[2], and Samuli Launiainen[3]

[1]Water, Energy and Environmental Engineering Research Unit, University of Oulu, Oulu, Finland
[2]Univ. Grenoble Alpes, Université de Toulouse, Météo-France, CNRS, CNRM, Centre d'Études de la Neige, Grenoble, France
[3]Bioeconomy and Environment, Natural Resources Institute Finland, Helsinki, Finland
[4]WSL Institute for Snow and Avalanche Research SLF, Davos, Switzerland
[5]Climate System Research, Finnish Meteorological Institute, Helsinki, Finland
[6]Institute for Atmospheric and Earth System Research INAR, University of Helsinki, Helsinki, Finland
[7]CNRM, Université de Toulouse, Météo-France, CNRS, Toulouse, France

Correspondence: Jari-Pekka Nousu (jari-pekka.nousu@oulu.fi)

Abstract. The snowpack has a major influence on the land surface energy budget. Accurate simulation of the snowpack energy and radiation budget is challenging due to e.g. effects of vegetation and topography, and limitations in the theoretical understanding of turbulent transfer in the stable boundary layer. Studies that evaluate snow, hydrology and land surface models against detailed observations of all surface energy balance components at high latitudes are scarce. In this study, we compared different configurations of SURFEX land surface model against surface energy flux, snow depth and soil temperature observations from four eddy covariance stations in Finland. The sites cover two different climate and snow conditions, representing the southern and northern subarctic zones, and the contrasting forest and peatland ecosystems typical for the boreal landscape. We tested different turbulent flux parameterizations implemented in the Crocus snowpack model. In addition, we examined common alternative approaches to conceptualize soil and vegetation, and assessed their performance in simulating surface energy fluxes, snow conditions and soil thermal regime. Our results show that a stability correction function that increases the turbulent exchange under stable atmospheric conditions is imperative to simulate sensible heat fluxes over the peatland snowpacks, and that realistic peat soil texture (soil organic content) parameterization greatly improves the soil temperature simulations. For accurate simulations of surface energy fluxes and snow/soil conditions in forests, an explicit vegetation representation is necessary. Moreover, we demonstrate the high sensitivity of surface fluxes to a poorly documented parameter involved in snow cover fraction computation. Although we focused on models within the SURFEX platform, the results have broader implications for choosing suitable turbulent flux parameterization and model structures depending on the potential use cases for high-latitude land surface modelling.

1 Introduction

The boreal zone, characterized by a mosaic of seasonally snow-covered peatlands, forests and lakes, is the largest land biome in the world. Snow conditions in the boreal zone are rapidly changing due to climate warming, which is found to be the strongest during the cold seasons in the Arctic (Serreze et al., 2009; Screen and Simmonds, 2010; Boisvert and Stroeve, 2015; Rantanen et al., 2022). Evidently snow has an important role for water resources and human activities in the cold regions, but it is also known that the snowpack characteristics affect animal movement (Tyler, 2010; Pedersen et al., 2021) and plant distribution (Rasmus et al., 2011; Kreyling et al., 2012; Rissanen et al., 2021). Recent studies show that especially cold-dwelling species have been shifting towards higher latitudes and altitudes in search for more suitable habitats (Tayleur et al., 2016; Couet et al., 2022). Therefore, the rapid warming of the Arctic, and its consequences on the quantity and properties of snow may define the destiny of many species and human activities in the boreal region. To predict future snow conditions, environmental change, and the consequences for water resources, ecosystems and people, predictive and process-based models possess great potential (Clark et al., 2015; Boone et al., 2017). Land surface models (LSMs) have been used for decades in numerical weather prediction and in global circulation models (Douville et al., 1995; Niu et al., 2011; Lawrence et al., 2019), and have more recently become common tools for interdisciplinary impact studies (Blyth et al., 2021).

Snowpack has a major impact on the wintertime energy budget due to its influence on the land surface albedo (hereafter albedo) and the surface heat fluxes (Cohen and Rind, 1991; Eugster et al., 2000). The heat diffusion within the snowpack is determined by the surface heat fluxes, internal properties of the snowpack and soil thermal regime. Correctly representing the snowpack is thus essential for simulating energy and mass exchange between the snow surface and the atmosphere, as well as below the snowpack (e.g. surface temperatures and soil freezing/thawing dynamics, Koivusalo and Heikinheimo, 1999; Slater et al., 2001). The snowpack energy budget is partitioned into downward and upward shortwave and longwave radiation, turbulent fluxes of sensible and latent heat, snowpack-ground heat flux and phase-changes in the snow. The snowpack energy balance and energy partitioning among the flux components vary strongly across diurnal and seasonal timescales, and between different ecosystems (Clark et al., 2011; Stiegler et al., 2016; Stigter et al., 2021). It is essential that LSMs are able to correctly reproduce this variability.

On the vast boreal and arctic peatlands with shallow vegetation, the snow cover can exclusively determine the wintertime albedo (Aurela et al., 2015). With minimal solar radiation during winter months on these open snow fields, turbulent fluxes make an important component in the energy budget of the snowpack, as they compensate the radiative cooling processes and further contribute to snow melt (Lackner et al., 2021; Conway et al., 2018). Simulation of turbulent fluxes under stable atmospheric conditions is known as one of the major sources of uncertainty in snow models (Lafaysse et al., 2017; Menard et al., 2021). In LSMs the turbulent fluxes are commonly computed with bulk aerodynamic approaches, where sensible and latent heat fluxes are proportional to the turbulent exchange coefficient according to the Monin-Obukhov similarity theory. These approaches typically use atmospheric stability correction functions based either on the bulk Richardson number (Martin and Lejeune, 1998; Lafaysse et al., 2017; Clark et al., 2015) or the Obukhov length scale (Jordan et al., 1999). It is established that the Monin-Obukhov similarity theory does not well represent low-wind and stable atmospheric conditions above aerodynam-

ically smooth surfaces such as snow (Conway et al., 2018). In such conditions, the simulated surface temperatures have been found to be unrealistically low, as the turbulent boundary layer tends to decouple from the snow surface (Derbyshire, 1999; Andreas et al., 2010). To circumvent this effect, stability correction functions have been modified to permit turbulent fluxes above critical stability thresholds (Lafaysse et al., 2017), by manipulating the wind speed (Martin and Lejeune, 1998; Andreas et al., 2010), or including a windless turbulent exchange coefficient (Jordan et al., 1999). Evaluations of these modifications often rely on validation with observed surface temperatures and snow depths (e.g. for the detailed snowpack model Crocus; Martin and Lejeune, 1998; Lafaysse et al., 2017) while comparisons against turbulent energy flux data remain scarce (Lapo et al., 2019; Conway et al., 2018).

The energy budgets of forest canopies and below-canopy snowpack are different to those on open peatlands, as turbulent exchange is attenuated by the canopy, and the snowpack energy budget and snow melt are mostly driven by the radiation balance (Rutter et al., 2009; Essery et al., 2009; Varhola et al., 2010). However, due to heterogeneous canopy structures and canopy processes (radiation transmittance, snow interception and unloading) together with low solar angles, the albedo dynamics of seasonally snow-covered boreal forests is complex (Malle et al., 2021). The absorption of the shortwave radiation can be highly heterogeneous, having direct implications on canopy temperatures (Webster et al., 2017), and on the resulting longwave radiative fluxes between canopy, snowpack and the atmosphere (Mazzotti et al., 2020b). Forest snow modelling has been identified as a priority in advancing cold region climate and hydrological models (Rutter et al., 2009; Krinner et al., 2018; Lundquist et al., 2021). Various models that have been proposed to represent the large-scale impact of forest on the snowpack energy budget (Niu et al., 2011; Lawrence et al., 2019; Boone et al., 2017) are still prone to large errors, due to the complexity and unresolved spatial scales of the underlying physical processes (Loranty et al., 2014; Thackeray et al., 2019). The forest snow model evaluations against concurrent snowpack and surface energy balance data are also surprisingly scarce. For instance, the explicit forest scheme of SURFEX LSM, MEB (Boone et al., 2017) has so far been evaluated only against data from three neighbour sites in Saskatchewan, Canada (Napoly et al., 2020). This considerably limits knowledge of the model skill to represent snow-forest interactions in regional or global applications.

The texture and thermal properties of the underlying soil can strongly impact the snowpack-ground heat exchange, snowpack energy fluxes and snowpack dynamics (Decharme et al., 2016). Peatlands have high soil organic content (SOC) and are characterized by high porosity, shallow water table, weak hydraulic suction, strong gradient in hydraulic conductivity from high values at the top to low values at the subsurface, low thermal conductivity, and large heat capacity (Decharme et al., 2016; Marttila et al., 2021; Morris et al., 2022; Menberu et al., 2021). These properties result in a wet soil profile resistant to temperature variations, while the drier top peat and moss layer can also provide effective insulation particularly during summertime (Beringer et al., 2001; Park et al., 2018; Chadburn et al., 2015). The importance of the soil texture is still often overlooked even in detailed snow models. For instance, in model comparisons of the ESM-SnowMIP project (Ménard et al., 2019), no SOC information was used to parameterize the participating LSMs to the reference sites. In addition, many spatial snow simulations neglect peat soils or SOC altogether, and their hydrological and thermal characteristics are derived from fractions of sand, silt and clay (Vernay et al., 2022; Brun et al., 2013; Mazzotti et al., 2021; Richter et al., 2021)

The goal of this study is to evaluate the ability of SURFEX LSM (Masson et al., 2013) to describe the surface energy balance and its drivers in boreal and subarctic peatlands and forests. We evaluate the effect of alternative turbulent exchange and snowpack parameterizations, and examine the skills of alternative model configurations to represent the soil-snow-vegetation interactions. The modelling framework includes flexible parameterizations for different processes within Crocus snowpack model (Vionnet et al., 2012), and its coupling to ISBA (Noilhan and Mahfouf, 1996; Decharme et al., 2016) and MEB (Boone et al., 2017; Napoly et al., 2017) models enable assessments of soil-snow-vegetation interactions. We compare the model simulations against observed surface energy fluxes, snow depth and soil temperatures from two forest and two peatland sites in Finland. We focus on the snow cover period, but cover also the snow-free season for a reference. At the peatland sites, we test the sensitivity of the surface heat fluxes to different turbulence and snow parameterizations, and assess how sensitive soil temperature and snowpack dynamics are to SOC. At the forest sites, we compare the simulations of ISBA composite soil-vegetation and MEB big-leaf forest scheme to assess the suitability of different forest-snow model structures.

2 Materials and methods

2.1 Study sites

We consider coniferous forest and peatland ecosystems in southern and northern Finland. Both areas are located in the boreal biome and have seasonal snow cover (Fig. 1, Table 1). Site photos can be found in the Supplement (Fig. S8).

2.1.1 Pallas Supersite (N-WET and N-FOR)

The Pallas area represents northern subarctic conditions, and is characterized by pine and spruce forests, wetlands, fells and lakes (Aurela et al., 2015; Lohila et al., 2015; Marttila et al., 2021). In this study, we use data from its two eddy-covariance (EC) flux stations.

Lompolojänkkä (northern peatland, N-WET) is a pristine northern boreal mesotrophic sedge fen where the wetter parts are dominated by sedges (*Carex rostrata* (most abundant), *Carex chordorrhiza*, *Carex magellanica* and *Carex lasiocarpa*) and the drier parts consist of shallow deciduous trees (*Betula nana* and *Salix lapponum*). Moreover, the fen has a fairly low coverage of shrubs, mainly *Andromeda polyfolio* and *Vaccinium oxycoccos*. The vegetation height is shallow ($\sim$0.4 m), with exception of isolated trees/bushes on the drier edges of the peatland.

Kenttärova (northern forest, N-FOR) is a northern boreal spruce forest, located on a hill-top plateau with mineral soil approximately 60 meters above Lompolojänkkä wetland. The forest is dominated by Norway spruce (*Picea abies*) with some deciduous trees, mainly birch (*Betula pubescens*) but also aspen (*Populus tremula*) and pussy willow (*Salix caprea*). According to the classification by Brunet (2020), Kenttärova is a sparse forest. Both sites and their measurements have been described in detail by Aurela et al. (2015).

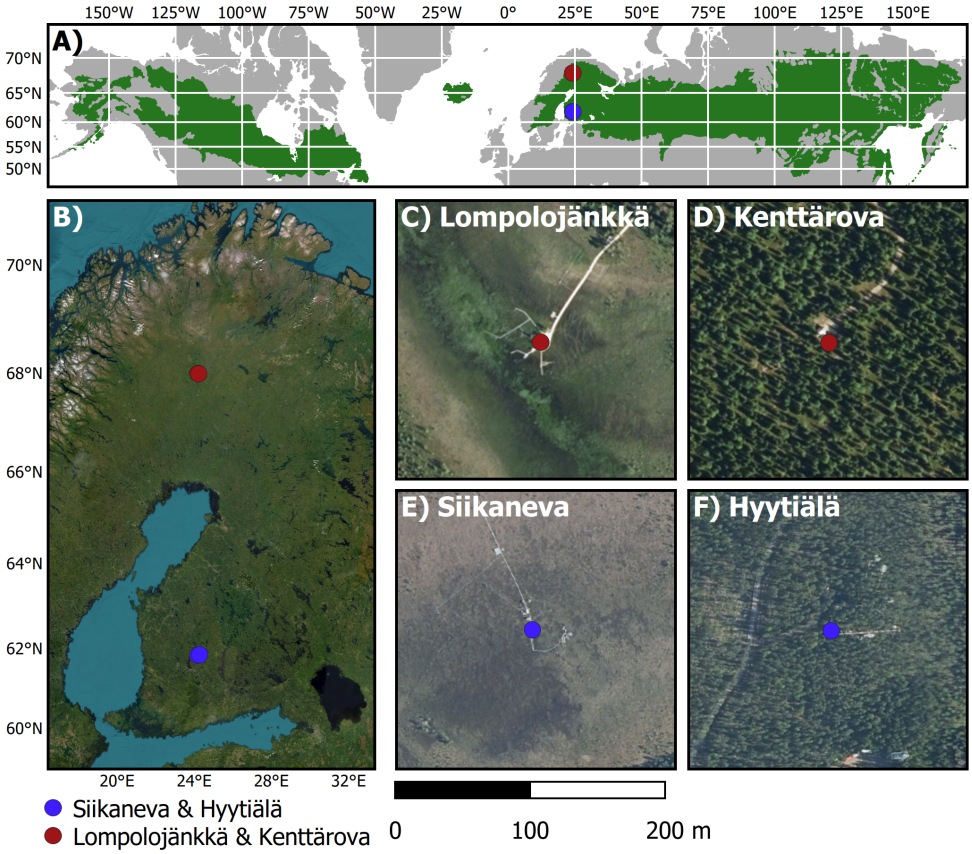

Figure 1. A) Study area locations inside the boreal land biome (green area, Olson et al., 2001), B) study site locations in Finland (Esri, 2023) and C-F) aerial images of each site (NLSF, 2020).

2.1.2 Hyytiälä and Siikaneva (S-WET and S-FOR)

The sites are located in southern subarctic conditions in the Pirkanmaa region in southern Finland, at about 5 km distance from each other. Siikaneva fen (southern wetland, S-WET) is a southern boreal oligotrophic fen dominated by sedges (*Eriophorum vaginatum*, *Carex rostrata* and *Carex limosa*), and has an extensive Sphagnum cover (mainly *Sphagnum balticum*, *Sphagnum majus* and *Sphagnum papillosum*). The site has been described in detail in Aurela et al. (2007); Alekseychik et al. (2017); Rinne et al. (2018).

Hyytiälä (southern forest, S-FOR) is a managed boreal Scots pine (*Pinus sylvestris*) dominated forest on mineral soil, described in detail by Launiainen (2010); Launiainen et al. (2022). According to the classification by Brunet (2020), the site is a dense forest.

Table 1. General site information.

Site	Code	Coordinates	Ecosystem	Soil type
Lompolojänkkä	N-WET	67°59.835' N, 24°12.546' E	mesotrophic fen	peat
Siikaneva	S-WET	61°49.961'N, 24°11.567'E	oligotrophic fen	peat
Kenttärova	N-FOR	67°59.237' N, 24°14.579' E	sparse spruce forest	podzol
Hyytiälä	S-FOR	61°50.471' N 24°17.439' E	dense pine forest	podzol

2.2 Models

We use components from the SURFEX LSM (Surface Externalisée, Masson et al., 2013) platform. SURFEX was selected as its modularity and vast range of model structures and incorporated process parameterizations enable its use in diverse applications. Specifically, we used ISBA (Noilhan and Planton, 1989; Noilhan and Mahfouf, 1996) for composite soil-vegetation, MEB (Boone et al., 2017; Napoly et al., 2017) for the canopy and Crocus (Vionnet et al., 2012) and its ensemble/multiphysics version ESCROC (Lafaysse et al., 2017) for the snowpack simulations. Specifically, ISBA coupled to Crocus is used for both peatland and forest experiments (Fig. 2A,B) whereas MEB coupled to Crocus is only used for the forest experiments (Fig. 2C). In the next subsections, we briefly describe these model components. Parameterizations and different configurations of ISBA, MEB and Crocus models are detailed in Sect. 2.3.

2.2.1 ISBA

ISBA (Interactions between the Soil, Biosphere and Atmosphere) is the soil and vegetation component of SURFEX (Noilhan and Planton, 1989; Noilhan and Mahfouf, 1996). It simulates the mass and energy fluxes in the soil-vegetation composite, as well as the exchanges between the soil-vegetation and the overlying atmosphere/snowpack (Fig. 2A,B). ISBA is used for the general circulation models by Meteo-France (Mahfouf et al., 1995; Douville et al., 1995; Salas-Mélia et al., 2005; Voldoire et al., 2013, 2019) and for numerical weather prediction in numerous countries (e.g. Hamdi et al., 2014; Bengtsson et al., 2017).

In ISBA, the surface heat flux between the atmosphere and the soil-vegetation composite (G_0, $\mathrm{Wm^{-2}}$) is computed as the residual of the sum of all surface/atmosphere energy fluxes:

$$G_0 = SWD(1 - LSA) + \epsilon(LWD - \sigma T_s^4) + H + LE \quad (1)$$

where SWD ($\mathrm{Wm^{-2}}$) and LWD ($\mathrm{Wm^{-2}}$) are the incoming shortwave and longwave radiations, respectively. The land surface albedo is denoted as LSA, ϵ is the surface emissivity, σ is the Stefan-Boltzman constant and T_s (K) is the surface temperature. The sum of the radiation terms is hereafter denoted as R_n ($\mathrm{Wm^{-2}}$).

The sensible heat flux H ($\mathrm{Wm^{-2}}$) is computed with the bulk aerodynamics approach:

$$H = \rho_a c_\rho C_H V_a (T_s - T_a) \quad (2)$$

where the air density, the specific heat capacity, the wind speed and air temperature are denoted with ρ_a ($\mathrm{kgm^{-3}}$), c_p, ($\mathrm{Jkg^{-1}K^{-1}}$), V_a ($\mathrm{ms^{-1}}$) and T_a (K), respectively. C_H is the turbulent exchange coefficient described later and is one of the parameters that is the focus of this study. When the soil is not fully covered by snow, the latent heat flux LE ($\mathrm{Wm^{-2}}$) is the sum of evaporation from the bare soil surface, E_g, evaporation of intercepted water on the canopy, E_c, transpiration from the vegetation, E_{tr}, and sublimation from bare soil ice, S_i:

$$LE = L_v(E_g + E_c + E_{tr}) + (L_f + L_v)(S_i) \tag{3}$$

where L_v ($\mathrm{Jkg^{-1}}$) and L_f ($\mathrm{Jkg^{-1}}$) are the latent heat of vaporization and fusion, respectively. Total evapotranspiration (ET) is computed as:

$$ET = E_g + E_c + E_{tr} = (1 - veg)\rho_a C_H V_a[h_u q_{sat}(T_s) - q_a] + veg\rho_a C_H V_a h_v \tag{4}$$

where veg is the fraction of vegetation cover, $\mathrm{q}_{sat}(T_s)$ ($\mathrm{kgkg^{-1}}$) is the saturated specific humidity at the surface, $q_a(T_s)$ ($\mathrm{kgkg^{-1}}$) is the atmospheric specific humidity, h_u is the dimensionless relative humidity at the ground surface related to the superficial soil moisture content and h_v is the dimensionless Halstead coefficient describing the E_c and E_{tr} partitioning between the leaves covered and not covered by intercepted water (see Noilhan and Mahfouf (1996) for details)

The turbulent exchange coefficient C_H is based on the formulation of Louis (1979):

$$C_H = \left[\frac{k^2}{ln(z_u/z_{0t})ln(z_a/z_{0t})}\right] f(R_i) \tag{5}$$

where z_u (m) is the reference height of V_a, z_a (m) is the reference height of T_a and humidity, z_{0t} (m) is the roughness height for heat, k (-) is the von Karman constant and $f(R_i)$ (-) describes the decrease of C_H as a function of increasing atmospheric stability, represented through Richardson number (R_i) (Louis, 1979).

Instead of separate treatment of the vegetation canopy and ground, ISBA considers the composite soil-vegetation energy budget (Fig. 2A,B). In the most detailed soil scheme ISBA-Diffusion (ISBA-DIF, Boone et al., 2000; Decharme et al., 2011), used in this study, 1D Fourier law is used to solve the soil heat diffusion, while a mixed-form Richards equation is applied for the 1D soil water movements. Similar as in Napoly et al. (2020), we use the $A - g_s$ stomatal conductance formulation derived from the coupling of photosynthetic CO_2 demand and stomatal function (Calvet et al., 1998).

ISBA uses parameters such as one-sided leaf area index (LAI, $\mathrm{m^2m^{-2}}$), vegetation height, vegetation thermal inertia, albedos of soil and vegetation, fractions of sand and clay as well as SOC content to characterize the composite soil-vegetation column. These parameters may be defined by the user, or obtained from global or regional databases (e.g. Faroux et al., 2013) and pedotransfer functions (Noilhan and Mahfouf, 1996; Peters-Lidard et al., 1998). In the presence of full snow cover, the surface energy budget is solved by Crocus (Sect. 2.2.3). For partial snow cover, Crocus is used to solve the snow covered fraction while the energy balance of the snow-free fraction is computed by ISBA, and total surface energy fluxes are computed as weighted averages of the snow and snow-free fractions (Sect. 2.3.1).

2.2.2 MEB

MEB (Multi-Energy Balance) is a recent ISBA development to explicitly describe vegetation and soil energy and mass balances. It was developed initially for forests (Boone et al., 2017; Napoly et al., 2017) and found to yield improved snow and soil temperature simulations (Napoly et al., 2020) but has not been evaluated for boreal and subarctic conditions. MEB simulates surface energy budget separately for soil and vegetation canopy. When the ground is snow covered, the energy budget of the snowpack is also explicitly represented. We used the MEB option, where the forest floor is covered by a litter layer instead of the bare soil surface (Napoly et al., 2020) (Fig. 2C). MEB describes vegetation canopy as a single big leaf (Boone et al., 2017). The respective energy balance equations for the canopy, the snowpack and the ground surface/litter layer in MEB are:

$$\begin{cases} C_v \frac{\partial T_v}{\partial t} = R_{nv} - H_v - LE_v + L_f \phi_v \\ C_{g,1} \frac{\partial T_{g,1}}{\partial t} = (1-\rho_{sng})(R_{ng} - H_g - LE_g) + \rho_{sng}(G_{gn} + \tau_{n,Nn} SW_{nn}) - G_{g,1} + L_f \phi_{g,1} \\ C_{n,1} \frac{\partial T_{n,1}}{\partial t} = R_{nn} - H_n - LE_n - \tau_{n,1} SW_{nn} + \epsilon_{n,1} - G_{n,1} + L_f \phi_{n,1} \end{cases} . \quad (6)$$

where C_v, $C_{g,1}$, $C_{n,1}$ ($\mathrm{Jm^{-2}K^{-1}}$) and T_v, $T_{g,1}$, $T_{n,1}$ K are the effective heat capacities and temperatures of the canopy, ground surface/litter layer and snowpack, respectively. In these equations, the subscripts $g,1$ and $n,1$ represent the uppermost layer for the soil and the snowpack, respectively. $G_{g,1}$ and $G_{n,1}$ are respectively the conduction heat flux at the bottom of the uppermost soil or snow layer. G_{gn} is the conduction heat flux at the soil-snow interface. R_{nv}, R_{ng}, R_{nn} ($\mathrm{Wm^{-2}}$) are net radiation, i.e. the sum of net shortwave radiation and net longwave radiation from/to the corresponding layer. The shortwave radiation scheme used in MEB is described in Carrer et al. (2013). Light transmission through the canopy is computed with a so-called sky view factor, which depends on LAI, solar angle and a vegetation dependant -constant (see Eq. 45 in Boone et al., 2017). H and LE flux parameterization as well as the stability correction functions are detailed in Boone et al. (2017). Obviously T_v, $T_{g,1}$, $T_{n,1}$ are also involved in the radiative and turbulent terms, providing a linear system of equations to be solved by an implicit numerical scheme. In this study, MEB is coupled to the ISBA-DIF soil scheme (Sect 2.2.1) and the snowpack model Crocus (Sect. 2.2.3). Energy fluxes between the canopy and the ground surfaces are calculated within MEB, and prescribed as upper boundary conditions in the subsequent Crocus and ISBA-DIF calculations.

2.2.3 Crocus

Crocus is a 1D physically based multilayer snowpack model (Vionnet et al., 2012). It is the most detailed snow scheme in ISBA, and has been used for operational avalanche hazard forecasting in the French mountain ranges for the past three decades (Morin et al., 2020). It aims to mimic the vertical layering of snowpacks with a Lagrangian discretization system, avoiding the aggregation of snow layers with highly different physical properties. A detailed description of Crocus and its integration in SURFEX can be found in Vionnet et al. (2012).

The snowpack surface energy budget is the sum of net radiation, turbulent fluxes and advective fluxes from precipitation. Over the snow, the sensible heat flux is computed similarly as in ISBA (Eq. 2) for soil surface, while the latent heat flux

(sublimation/deposition), LE_s, is computed as:

$$LE_s = (L_f + L_v)\rho_a C_H V_a[q_{sat}(T_s - q_a)], \tag{7}$$

where T_s (K) is the snow surface temperature. The bottom of the snowpack and the uppermost soil layer of ISBA are fully coupled with a mass and energy conserving semi-implicit solution. The semi-implicit solution refers to a coupled system in which both components are solved separately with an implicit approach considering that the state of the second system remains constant during the solving of the first system. The heat conduction flux G_{gn} at the snow-soil interface is explicitly computed using the Fourier equation, and depends on the temperature gradient between the bottom snow layer and the uppermost soil layer (Eq. 4 in Decharme et al., 2011). The soil thermal conductivity and heat capacity are described using pedotransfer functions of ISBA (Noilhan and Mahfouf, 1996; Peters-Lidard et al., 1998).

2.3 Model configurations and parametrization

2.3.1 Model configurations

We use three different configurations of ISBA, MEB and Crocus modules (Fig. 2). The first two configurations use the composite soil-vegetation conceptualization of ISBA (Fig. 2A,B), and differ only in how the snow cover fraction is represented. ISBA aggregates the properties of soil and vegetation depending on vegetation fraction (veg) that covers a given grid-cell.

The first configuration (referred as ISBA-FS) assumes the snowpack to fully cover the soil-vegetation composite regardless of the snow depth (Fig. 2A). It is the common approach for snow simulations over shallow vegetation or bare soil (Vernay et al., 2022; Nousu et al., 2019), for large-scale reanalyses (Brun et al., 2013) and some hydrological applications (Lafaysse et al., 2011; Revuelto et al., 2018). In addition, most site-level evaluations of SURFEX snow schemes rely on ISBA-FS configuration (Decharme et al., 2016; Lafaysse et al., 2017).

In the second configuration (referred as ISBA-VS), a part of the soil-vegetation composite is covered by snow while the remaining (non-snow) fraction stays in constant contact with the atmosphere. This proportion is governed by snow depth. The effective snow cover fraction is the weighted average between the snow fraction of vegetation (p_{snv}) and snow fraction of the bare ground (p_{sng}), calculated as (Decharme et al., 2019; Napoly et al., 2020):

$$p_{snv} = min(1.0, \frac{HS}{HS + w_{sw} z_0}) \tag{8}$$

$$p_{sng} = min(1.0, \frac{HS}{HS_g}) \tag{9}$$

where HS (m) is the snow depth, HS_g is the threshold value for snow depth (0.01 m by default), and z_0 (m) denotes the surface roughness. The coefficient w_{sw} is supposed to relate to scale-dependent vegetation characteristics and is assigned as 5 by default in SURFEX and in numerical weather prediction configurations (as well as in this study). However, without clear

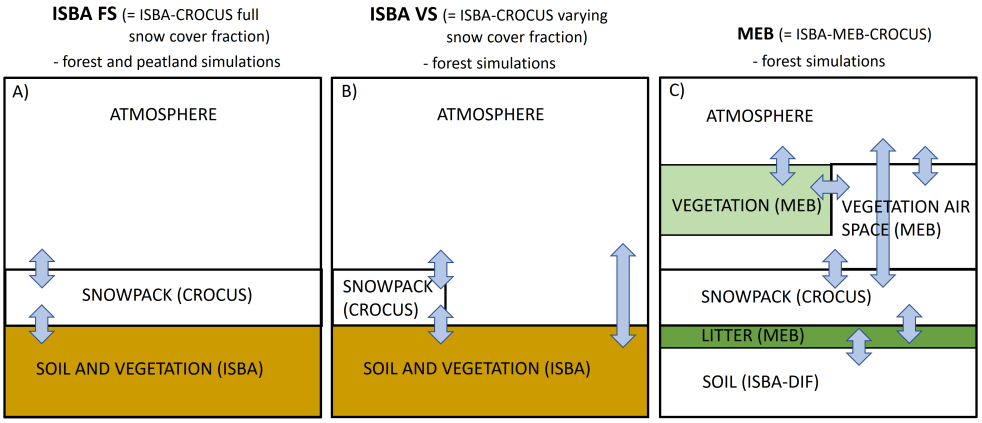

Figure 2. Three different model configurations used in the study: (A) ISBA-FS with full snow cover fraction, (B) ISBA-VS with varying snow cover fraction, and (C) MEB big-leaf approach. Considered energy fluxes between domains are represented with arrows.

consistency, highly different values of w_{sw} have been used e.g. in climate simulations (w_{sw} = 2 by Decharme et al., 2019) and hydrological applications (w_{sw} = 0.2 by Le Moigne et al., 2020). We present a summary of the application specific treatment of the snow cover fraction and w_{sw} in the Appendix (Table C1). This summary shows that selection of w_{sw} value seems arbitrary and the fractional concept is only loosely linked to any physical relationships between soil, vegetation and snow. Yet, it is necessary for such a composite approach.

The third configuration (later denoted as MEB) is the big-leaf approach where the fluxes between the canopy and snowpack/ground are explicitly computed by MEB, and prescribed in the subsequent Crocus snowpack and ISBA-DIF soil modules (Fig. 2C).

2.3.2 ESCROC parameterizations for snow processes and turbulent exchange

We use the multiphysics version of Crocus (ESCROC, Ensemble System Crocus, Lafaysse et al., 2017) to evaluate the impact and associated uncertainties of the different parameterizations of snow processes and turbulent exchange. In ESCROC, the main physical processes and properties of snowpack, as well as the turbulent fluxes, can be represented by several alternative options. These include density of new snow, snow metamorphism, absorption of solar radiation, turbulent fluxes, thermal conductivity, liquid water holding capacity, snow compaction and surface heat capacity (Eqs. 1-17 in Lafaysse et al., 2017). Lafaysse et al. (2017) showed that an optimized standard subensemble of 35 members (E_2 subensemble) is sufficient to provide a spread of the appropriate magnitude compared to model errors. We use this subensemble (hereafter ESCROC-E_2) similar to recent studies quantifying the model uncertainty (e.g. Deschamps-Berger et al., 2022; Tuzet et al., 2020). The presented ensemble spread correspond to simulated values between ensemble minimum and maximum.

In Crocus, the default turbulent exchange parameterization (Eq. 5) has been found to underestimate the turbulent fluxes under stable conditions (Martin and Lejeune, 1998). Therefore, different stability dependencies of the C_H have been implemented in ESCROC-E_2. They differ mainly in the R_i thresholds below which C_H is assigned a constant value to enable turbulent heat and mass transport under stable conditions. As shown by Fig. 4 in Lafaysse et al. (2017), these parameterizations are a) classical Louis (1979) formula (later referred as RIL) with threshold at R_i = 0.2, b) RIL with threshold at R_i = 0.1 (RI1), c) RIL with threshold at R_i = 0.026 (RI2), and d) modified formulation with effective roughness length for heat (10^{-3}m), minimum wind speed (0.3 ms^{-1}), and with threshold at R_i = 0.026 (M98) by Martin and Lejeune (1998). The RIL parameterization is widely used in SURFEX applications (e.g. Decharme et al., 2019; Le Moigne et al., 2020), RI2 is applied in operational snow modelling in the Alpine area (Vernay et al., 2022), and M98 was recently used in the Canadian Arctic by Lackner et al. (2021). However, evaluations of the different Crocus turbulent flux parameterizations against surface flux data are still lacking. MEB uses a different stability correction term (Boone et al., 2017) and applies only the RIL option for the stable conditions.

2.3.3 Site parameters

The parameterization of ISBA and MEB for the study sites is given in Table 2. Summer LAI and vegetation height were obtained from literature, while winter LAI (and monthly LAI cycle) was estimated according to the proportion of deciduous and coniferous vegetation on each site. The LAI of S-FOR refers to conditions before forest thinning in early 2020. The thinning, resulting in ca. 35% reduction in LAI, was neglected in our simulations as major part of the simulation period covers time before the thinning. Vegetation types in ISBA are characterized according to ECOCLIMAP (Champeaux et al., 2005); the forest sites in this study classify as boreal needleleaf evergreen, while the peatland sites are best represented as boreal grass. Additional parameters based on LAI, vegetation height and vegetation type are computed following the standard methods of ISBA (Noilhan and Mahfouf, 1996; Carrer et al., 2013).

Soil texture (sand and clay fractions) for the forest sites are based on *in situ* measurements. The peat soils at S-WET and N-WET were parameterized as fully organic for the uppermost 1 m, in accordance with field measurements (Väliranta and Mathijssen, 2021; Muhic et al., 2023), while the deeper layers were assigned as mineral soil similar to the contiguous forests. Although peat profiles may be deeper, the soils below the damping depth of annual temperature fluctuations (ca 1.1 m for saturated peat soil with porosity ca 90 %) are assumed not to have significant impact on surface energy flux dynamics. The SOC values for mineral soils of N-FOR and S-FOR were taken from Lindroos et al. (2022). The rest of the parameters presented in Table 2 were assigned as estimates. The thermal and water retention parameters are subsequently derived from the pedotransfer functions of ISBA (Noilhan and Mahfouf, 1996; Peters-Lidard et al., 1998).

Table 2. Main model parameters for the study sites. Vegetation types BOGR and BONE correspond to boreal grass and boreal needleleaf evergreen, respectively.

Parameter	N-WET	S-WET	N-FOR	S-FOR	Source
Veg. type	BOGR	BOGR	BONE	BONE	ECOCLIMAP: Champeaux et al. (2005)
Veg. fraction (only with ISBA-VS) (-)	0.95	0.95	0.95	0.95	ECOCLIMAP: Champeaux et al. (2005)
Veg. height (m)	0.4	0.25	13	15	Aurela et al. (2015); Alekseychik et al. (2017) Kolari et al. (2022)
LAI_{max} (m^2m^{-2})	1.3	0.6	2.1	3.0	Aurela et al. (2015); Alekseychik et al. (2017) Kolari et al. (2022)
LAI_{min} (m^2m^{-2})	0.3	0.1	1.9	2.4	assigned
Veg. albedo (NIR/VIS) (-)	0.136	0.187	0.145	0.145	assigned
Soil albedo (NIR/VIS) (-)	0.136	0.187	0.145	0.145	assigned
Tair measurement height (m)	2	2	2	2	FMI (2021)
Wind measurement height (m)	13	3	23	16.8	Aurela et al. (2015); Mammarella et al. (2019) Alekseychik et al. (2022a)
Elevation (m)	270	162	347	181	Hari et al. (2013); Alekseychik et al. (2022a); FMI (2021)
Clay (%) (below 1 m at peatlands)	9	7	9	7	measurements
Sand (%) (below 1 m at peatlands)	76	65	76	65	measurements
SOC (0-30cm) (kgm^{-2})	93,5	93,5	3.0	3.5	Lindroos et al. (2022) Muhic et al. (2023); Väliranta and Mathijssen (2021)
SOC (30-70cm) (kgm^{-2})	93,5	93,5	1.75	0.75	Lindroos et al. (2022) Muhic et al. (2023); Väliranta and Mathijssen (2021)
SOC (70-100cm) (kgm^{-2})	93,5	93,5	0	0	Väliranta and Mathijssen (2021); Muhic et al. (2023)
Start of simulation (yyyy-mm)	2013–09	2016–09	2013–09	2008–09	-
End of simulation (yyyy-mm)	2021–07	2021–07	2021–07	2021–07	-

2.4 Data

2.4.1 Model forcing

Meteorological forcing consist of hourly observations of air temperature, wind speed, precipitation rate, air humidity, downward shortwave and longwave radiation and atmospheric pressure. The available meteorological observations from the nearest meteorological stations were obtained from Finnish Meteorological Institute (FMI) open database (FMI, 2021) (Station IDs: N-WET 778135, N-FOR 101317, S-FOR 101987). Meteorological observations at the S-WET site come from the SMEAR database (Alekseychik et al., 2022a). At S-WET and S-FOR the shortwave and longwave radiation were obtained from the SMEAR database, while at N-WET and N-FOR data from FMI stations were used. The diffuse to total shortwave radiation ratio, r, was estimated as a function of the cosine of the sun zenith angle, μ. More specifically, a 3rd degree polynomial fit

between r and μ was obtained using the atmospheric model SBDART (Ricchiazzi et al., 1998) to simulate diffuse and total solar radiation in clear sky conditions. The atmospheric profile was set to typical winter conditions, 0.09 for the aerosol optical thickness, 300 DU for the ozone column and 0.854 gcm^{-2} for the water vapor column.

The data gaps in meteorological observations were first filled by the contiguous sites (e.g. N-FOR for N-WET and vice versa) and the remaining gaps by other nearby meteorological stations (IDs: N-WET/N-FOR 101932, S-WET/S-FOR 101520). The missing radiation observations were first filled by the contiguous sites, and the remaining gaps by ERA5 reanalysis data (Hersbach et al., 2020). Only less than 10 hours of ERA5 data was used for N-WET, N-FOR and S-WET. However, S-FOR radiation observations contained more gaps, specifically LWD in 2008–2012. A good agreement between site observations and ERA5 estimates of LWD is shown in Appendix (Fig. B1). Furthermore, fraction of snow to total precipitation $P_{ice}/(P_{ice}+P_{liq})$ is assumed to linearly decrease from 1 to 0 at air temperatures between 0°C and 1°C.

2.4.2 Model evaluation data

We use surface energy flux observations, snow depth and soil temperatures in model evaluation. The availability period of each variable is given in Table B1. On all sites, upward shortwave radiation (SWU) and upward longwave radiation (LWU) were measured using pyranometers and pyrgeometers, while ground heat flux (G) was measured using soil heat flux plates between 5 and 10 cm depths.

The sensible heat (H) and latent heat (LE) were measured by the eddy-covariance (EC) technique. The EC systems consist of USA-1 (METEK) three-axis and Gill HS-50 sonic anemometers as well as closed-path LI-7000 and LI-7200 (Li-cor, Inc.) CO_2/H_2O analysers. The detailed descriptions of the instrumentation, footprint analysis and the procedures for obtaining the turbulent heat fluxes from raw eddy covariance data is detailed in the original data and site publications (N-WET/N-FOR; Aurela et al. (2015), and S-WET/S-FOR; Mammarella et al. (2016, 2019); Alekseychik et al. (2022b). In short, the H and LE were screened for instrument failure and data outliers, and data was quality flagged according to friction velocity (u_*) and flux stationarity (FST) criteria (Foken et al., 2005):

- flag 2: all data (after screening of instrument failures and outliers)
- flag 1: $u_* \geq 0.1$ ms^{-1} and 0.3 $\leq$ FST $\leq$ 1.0
- flag 0: $u_* \geq 0.1$ ms^{-1} and FST $\leq$ 0.3

At S-WET, S-FOR and N-FOR, automated snow depth observations are directly used (FMI, 2021). On N-WET the automated snow depth measurement is at 0.7 m height, and therefore the exceeding snow depths were taken from biweekly manual measurements. To account for the spatial variability of snow depth in the forests, manual snow depth measurements from a snow course in the close proximity of the automated measurements were used (Aalto et al., 2022; Marttila et al., 2021). Each site has different configuration of soil temperature sensors. At N-FOR and N-WET stations, soil temperatures are measured at 5 and 20 cm depths (Aurela et al., 2015). Soil temperatures at S-FOR and S-WET are measured at depths of 0, 5, 10, 30, 50 and 75 cm (Aalto et al., 2022).

2.5 Model experiments

On the peatland sites, we evaluate the skill of ISBA-FS (Sect. 2.3.1) and effect of ESCROC-E_2 parameterizations (Sect. 2.3.2) on surface heat fluxes over snowpack and bare ground. The simulations are further used to assess the differences in snow depth simulations between ESCROC-E_2 turbulent exchange options. For a more detailed evaluation of two contrasting turbulent exchange options, we conducted deterministic ISBA-FS simulations with site parameters and default ESCROC-E_2 snow parameterizations, but different treatments of turbulent exchange; RIL and M98 options (see Sect. 2.3.2, referred as RIL-SOC and M98-SOC). Moreover, the influence of soil texture was explored by comparing M98-SOC to simulation where soil was parameterized as mineral, similar to the contiguous forest site (referred as M98-MIN).

On the forest sites, we examine the skills of the different alternatives to represent the energy and mass budgets of soil and vegetation (ISBA-VS, ISBA-FS, MEB in Sect. 2.3.1), and their implications on snow depth, soil temperature and surface energy fluxes. First, we compare ESCROC-E_2 simulations with these three configurations focusing on the snow depth and soil temperature. The ISBA-VS simulations are conducted with the default snow cover fraction parameterization (Eq. 8). For a more detailed comparison of the simulated and observed above-canopy surface energy fluxes by ISBA-VS and MEB, we conducted deterministic simulations with the default Crocus parameterizations (as in Fig 2. in Lafaysse et al. (2017)).

Model simulation periods for each site are in Table 2. For each site, the model initial state was obtained by a spin-up simulation from the start date (Table 2) to September 2020. In total of ca. 290 ensemble and deterministic simulations were conducted.

2.6 Model evaluation metrics

Time series of daily averages are used to represent the results, whereas mean absolute error (MAE), mean bias error (MBE) and coefficient of determination (R^2) are used in quantitative model-data comparison. To detect possible biases in model simulations, we use scatter plots and quantile-quantile plots of sorted observations against sorted simulations. The sign convention is so that the surface energy fluxes are presented relative to the surface (i.e. negative flux means that surface is losing energy). In time series, the turbulent flux observations include all EC data (Sect 2.4.2, quality flag ≤ 2). We demonstrate the results by using the winter season 2018–2019 as an example time series period thanks to its best coverage of energy flux data (least gaps), and typical snow conditions on all sites. For the scatter and quantile-quantile plots, only flux data with quality flag ≤ 1 is used, and the results computed as aggregated 6-hour means include periods where observations are available (referred later as evaluation period). We compare snow and snow-free conditions by grouping the results into time windows where models and observations agree of the ground conditions (snow or snow-free).

3 Results

3.1 Observed energy balance at peatland and forest sites

The energy budget at high-latitudes have a strong seasonal variation driven by solar radiation (Fig. 3). In winter (December, January, February), longwave radiation balance to large extent determines R_n, particularly in the northern Finland. Daily average R_n is negative down to -50 Wm^{-2} and lower, which implies considerable radiative cooling. Towards spring the radiation budget is gradually counterbalanced by shortwave radiation. On the peatlands, a large fraction of SWD is reflected during snow cover, and daily R_n turns positive in late melting season (Fig. 3A,C). At the forest sites, the timing of R_n becoming positive is less sensitive to the presence of snow, as a large proportion of SWD is absorbed by vegetation. In summer, high solar elevation and the absence of the reflective snow surface cause daily R_n to be up to 200 Wm^{-2}.

The R_n is balanced mostly by H and LE, and to a lesser extent snowpack/ground heat flux (Fig. 3). The residual line represents the amount of energy that would be required to close the observed energy budget (Fig. 3). It includes changes in internal energy of the snowpack and vegetation, but also reflects the common energy balance closure problem in EC-measurements (Mauder et al., 2020) (see Sect. 4.4). The energy balance closure in snow-free conditions was typical for EC-measurements, ranging from 0.81 to 0.99 (Mauder et al., 2020). The lack of snowpack heat flux and/or temperature profile measurements did not enable assessing the closure during snow cover periods. In winter, LE and G are small and the radiative cooling is counterbalanced mostly by downward H, corresponding to warming of the snowpack and/or vegetation, and cooling of the ambient air. The R_n during winter falls lower (more negative) on the northern sites, and thus also downward H becomes stronger (daily average up to 50 Wm^{-2}). In summer, both H and LE are negative (upward) heating the atmosphere, while downward G drives the warming of soil profile. At all sites, LE increases along the growing season and peaks approximately in July. In autumn, the turbulent fluxes decrease as response to reduced R_n.

3.2 Peatland simulations

The sensitivity of surface heat fluxes and snow depth to different ESCROC-E_2 model parameterizations is shown in Fig. 4. The spread corresponds to the difference between the minimum and maximum of the ensemble. Notably, H has relatively high spread, especially on N-WET, and the observed H often lies near the limit or even outside the simulated range at both S-WET and N-WET. Modelled wintertime LE is low and, as for H, the observed values are near the limit or outside the simulated range, especially in spring. LWU has strong day to day variation well captured by the model, and the spread is rather small relative to the total flux.

3.2.1 Impact of alternative turbulence (C_H) parameterizations

To assess the sensitivity of snow depth simulations to alternative turbulence parameterizations, and to alternative snow process options, we examined simulations where the ESCROC-E_2 members are grouped according to their turbulent flux option (Fig.

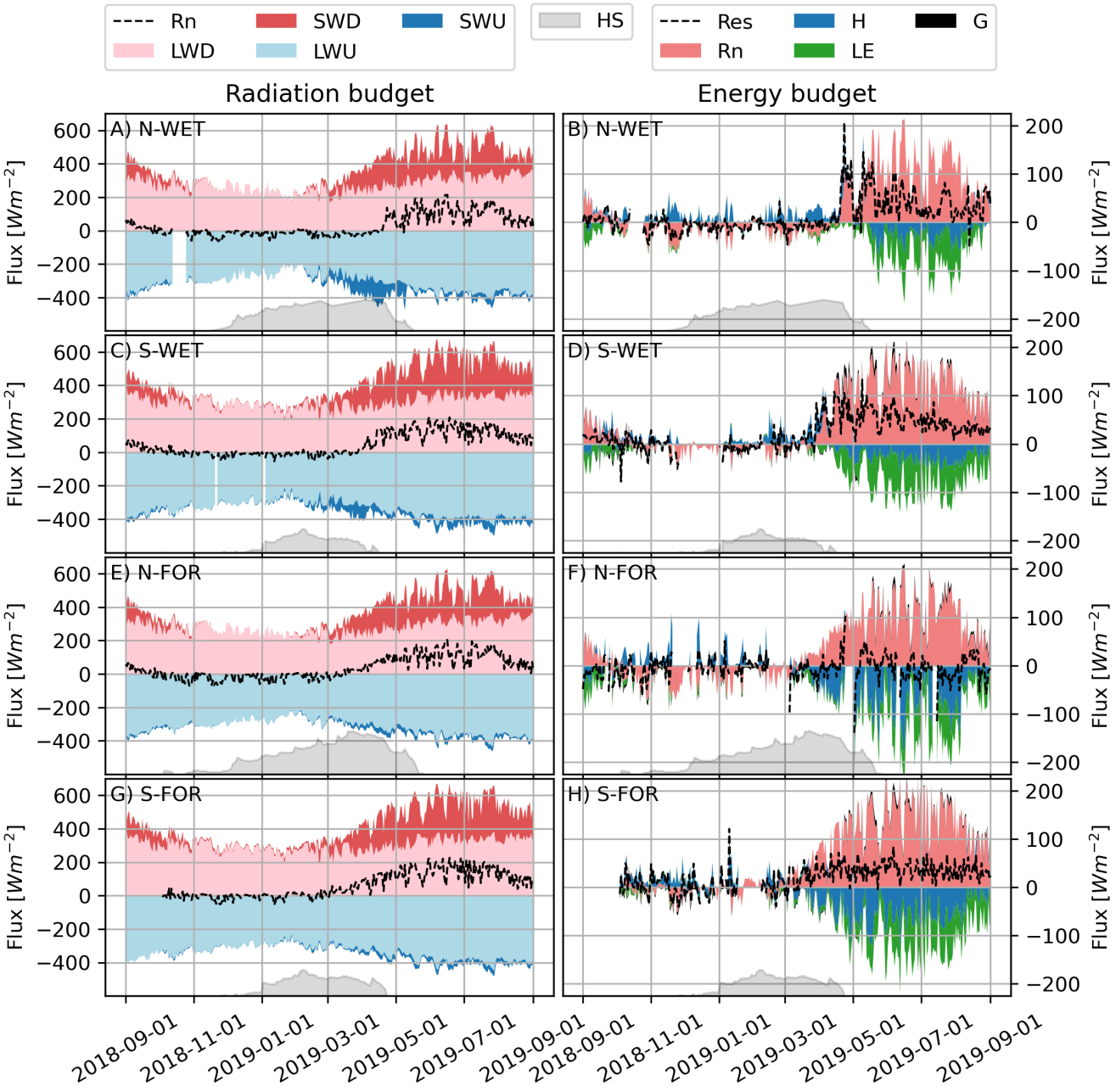

Figure 3. Observed daily averaged radiation budget (left) and surface energy budget (right) of hydrological year of 2018–2019. Colored stacks represent the observed fluxes relative to the surface as shown in legends (i.e. incoming fluxes are positive and outgoing fluxes negative). Dashed line in energy budget plot corresponds to the residual after the sum of each energy component whereas the dashed line in the radiation plot shows the net radiation (R_n). Note different scale in left and right columns. Ground heat flux (G) is missing on N-WET. The observed evolution of the snow depth (HS) is shown in gray polygon (not in scale).

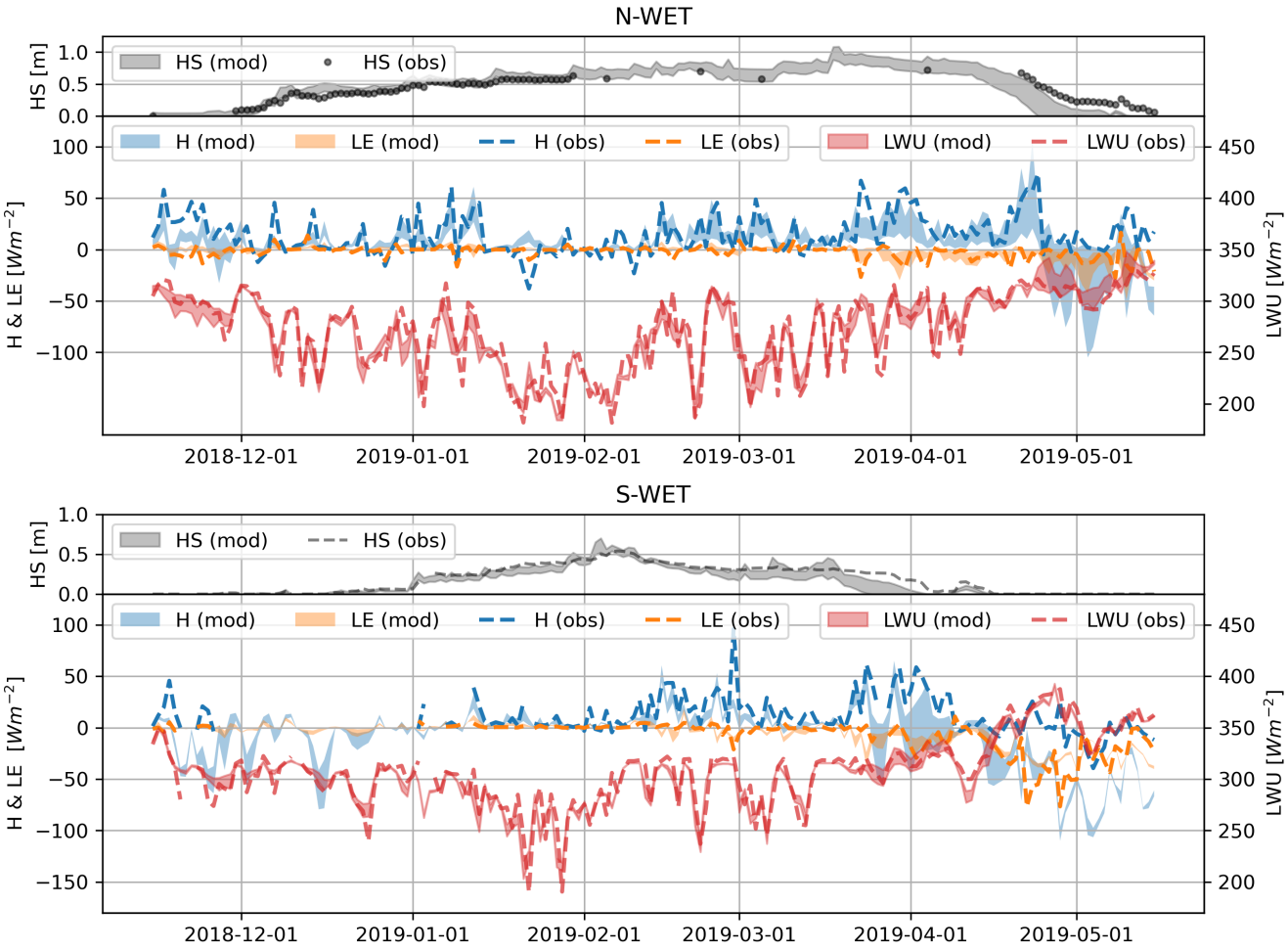

Figure 4. Time series of daily averaged surface heat flux spread simulated by ISBA-FS with ESCROC-E_2 35 ensemble members against corresponding observed values during 2018–2019 snow season. H, LE and LWU correspond to sensible heat, latent heat and upward longwave radiation fluxes, respectively. The observed and simulated evolution of snow depth (HS) are shown in gray.

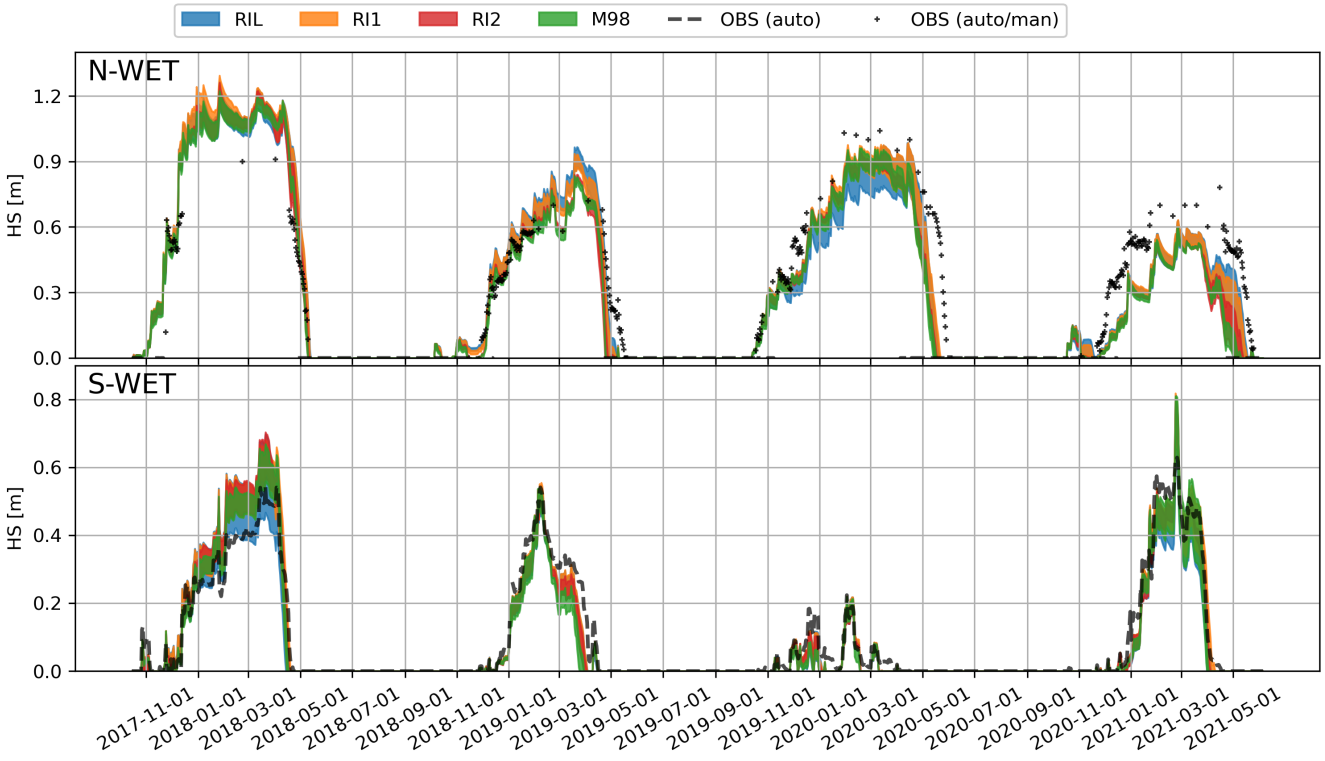

Figure 5. Time series of snow depths (HS) simulated by ISBA-FS ESCROC-E_2. The 35 ensemble members are grouped by their turbulent flux parameterization, and the spread of each group is presented in colored ranges. Observed snow depths are presented in black dots and dashed lines.

385 5). During snow accumulation periods, the spread is small and the groups are consistently overlapping on both sites, indicating that the differences in snow accumulation and maximum snow depth are driven mostly by the uncertainty of snow process descriptions. The spread increases during and after snow melt events, indicating higher importance of turbulent fluxes on snow melt dynamics. While it is difficult to identify a group that fits observed snow depths best, the winter melt event in 2018–2019 on N-WET is only captured by the M98 and RI2 parameterizations.

390 These findings are consistent with the comparison of simulated H and LWU by the two deterministic runs (RIL-SOC and M98-SOC) against observations (Fig. 6). With the RIL-SOC parameterization, the magnitude of H is largely underestimated, while this bias is to most extent corrected by using M98-SOC. Improved simulation of H and surface temperature also entail improved LWU (Fig. 6), but the modelled H fluxes still only moderately correlate (R^2) with observations. In terms of LE, the simulations are not improved by the M98-SOC (see Fig. S1), possibly due to low magnitude and high relative uncertainty of 395 wintertime LE over snow.

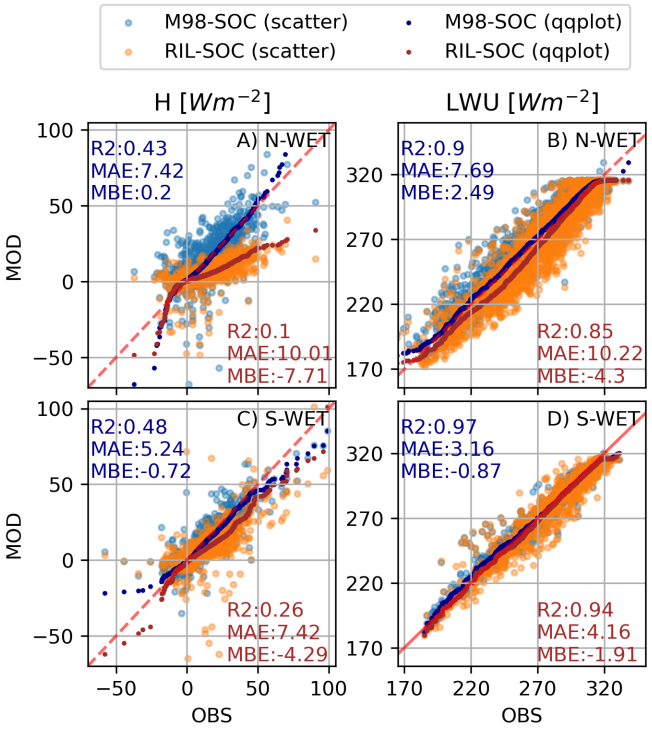

Figure 6. Scatterplots and quantile-quantile plots of sensible heat flux (H) and upward longwave radiation (LWU) during snow cover for the evaluation period with the RIL-SOC and M98-SOC turbulence parameterizations.

3.2.2 Radiative fluxes

We compare the simulated and observed albedo, SWU, LWU and surface temperatures with snow-free and snow conditions in Fig. 7. These experiments correspond to the deterministic M98-SOC simulation.

The modelled SWU generally matches the observations well, but the scatter increases with increasing SWD, indicating uncertainties in simulated albedo when shortwave forcing is high over the snowpack in spring. These cause a slight underestimation of simulated spring albedo, also visible in the time series especially on N-WET (Fig. 7). Moreover, simulated albedo tends to be overestimated during shallow snow depth both in spring and autumn. This is because the ISBA-FS approach assumes snow to completely cover the ground regardless of the snow depth, while in reality the fractional snow cover can lower the albedo. In contrast in May 2019, the underestimation of albedo on N-WET is due to an incorrect timing of snow melt (too early snow disappearance in the simulation). The mean absolute errors in simulating SWU are small and of similar magnitude (from $\sim$4 to 9 Wm^{-2}) both for snow and snow-free conditions.

Warmer surface temperatures during snow-free season result in higher LWU compared to winter and spring (Fig. 7). The surface temperatures and LWU are generally well simulated across sites and ground conditions at least with the presented time intervals. During snow cover, the upper tail of the radiation distribution is slightly higher than simulated; however the mean

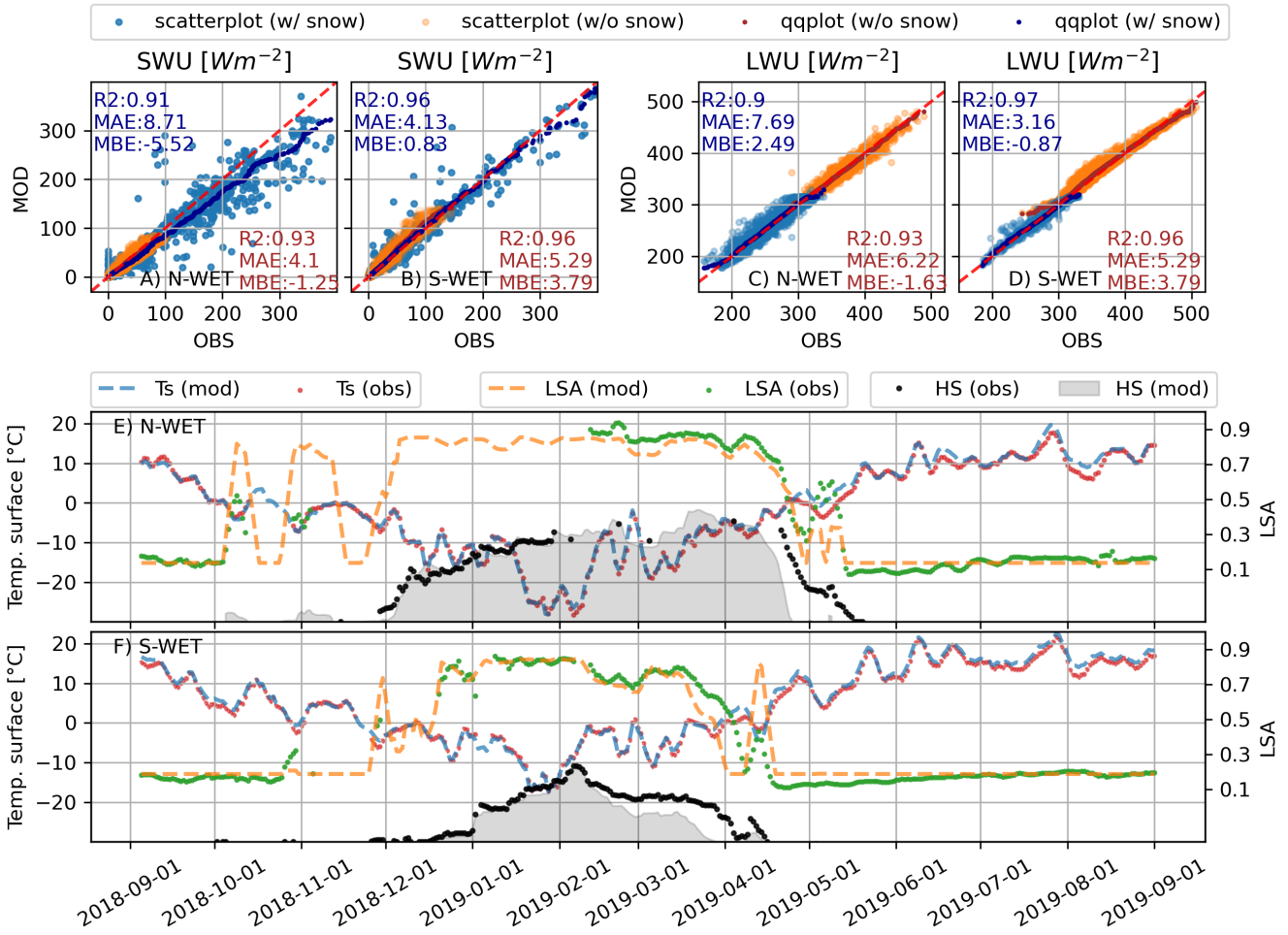

Figure 7. Scatter plots and quantile-quantile plots of modelled against observed upward shortwave radiation (SWU) (A,B) and upward longwave radiation (LWU) (C,D) on peatland sites with snow cover (w/ snow) and without snow cover (w/o snow) as well as the time evolution of 5-day rolling means of albedos (LSA) and surface temperature (Ts) as simulated and observed from September 2018 to September 2019 (E,F). The evolution of the snow depth (HS) is not in scale.

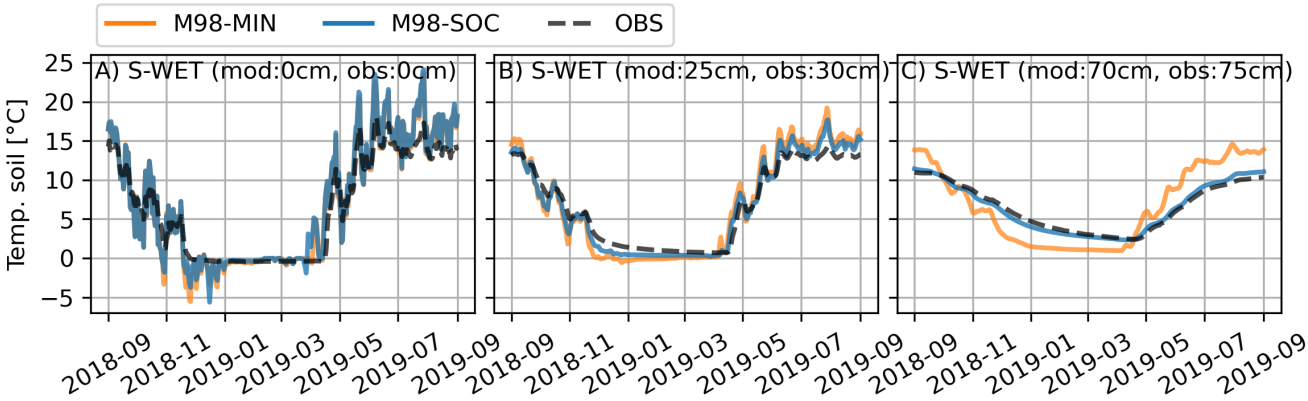

Figure 8. Effect of soil parameterization on soil temperatures (A-C) during a hydrological year at the S-WET site. M98-MIN refers to mineral soil and M98-SOC to peat soil. The observed soil temperatures are compared to the closest model layer; the depths of measurements and simulations are presented in each panel.

biases are generally very low. There are no other visible biases in LWU simulations and the other metrics are also very good, consistent with Fig. 4. The mean absolute errors in simulating LWU are similar for snow and bare ground ($\sim$3 to 8 Wm^{-2}).

3.2.3 Soil thermal regime

The effect of soil parameterization on simulated soil temperature dynamics at S-WET is shown in Fig. 8. Due to shallow water table, the soil profile remains nearly saturated throughout the year. As the porosity and field capacity in the M98-SOC parameterization are much higher than in the M98-MIN, the former has also significantly higher heat capacity and smaller thermal diffusivity. This means soil temperature variations are attenuated in M98-SOC compared to M98-MIN, and this attenuation becomes increasingly important in deeper soil layers (Fig. 8). The results show that including a realistic soil profile (SOC) greatly improves the peatland soil temperature simulations at depths 50–70 cm, but only slightly close to the surface (0–10 cm) (see Fig. S2 for comparisons of more soil depths). On both sites, the simulated surface soil temperature variations in summer are greater than observed. This is presumably because ISBA does not include the insulating moss/litter layer on top of the peat soil, as well as due to water table dynamics, potentially affected by lateral flows not accounted for. Due to the weak influence on the surface soil temperatures, the soil parameterization (M98-SOC vs. M98-MIN) does not significantly affect the simulated snow depth (Fig. S2).

3.3 Forest simulations

3.3.1 Impact of vegetation representation on snow depth

The three different vegetation representations (Sect. 2.3.1) have highly contrasted effect on the forest energy budget, snowpack, and soil temperature simulations. In general, the snowpack simulations for the forest sites are poorer than for the peatland sites; however the observed snow depths also vary considerably within the forests (see OBS in Fig. 9 and Sect. 4.4).

The simulated snow depth with the ISBA-VS (composite soil-vegetation and varying snow cover fraction, Fig. 2B) does not agree with the observations; the model version heavily overestimates accumulation on N-FOR in 2021 and predicts extremely rapid, strong and too early melt events (Fig. 9). Replacing the default snow cover fraction parameter (w_{sw} = 5) with w_{sw} = 0.2 (used for hydrological modelling in Le Moigne et al., 2020) yields slightly better snow depth dynamics for N-FOR, but the results remain unsatisfactory (Fig. C1 in the Appendix). The different sensitivity of w_{sw} parameter for S-FOR and N-FOR simulations is explored via soil temperature simulations in Fig. C2; With the default snow cover fraction parameter, particular warm events on N-FOR heat up the soil causing the snowpack to melt, while simulation with w_{sw} = 0.2 manages to retain freezing soil temperatures.

MEB (explicit canopy, ground and snowpack energy balance) simulates the snow accumulation periods at N-FOR very well but peak snow is reached too early and maximum snow depths are underestimated. This is due to combined impact of overestimated compaction and too early start and progression of the snow melt. The role of both processes was evident from comparison of modelled and observed snow water equivalent (see Fig. S6).

ISBA-FS performs better during the snow accumulation period, with simulated snow depths very close to observations. However, the ablation of snow is too rapid, and the final melt out dates are close to those simulated by MEB. On S-FOR, MEB captures both snow accumulation (including peak snow depths), melt dynamics and final melt out dates rather well. ISBA-FS predictions are generally close to MEB. As MEB only considers one option for turbulent exchange (RIL), the spread of the ensemble is smaller than for the ISBA configurations (Fig. 9). The uncertainties of other snow processes accounted for in ESCROC-E_2 are not sufficient to explain the discrepancies between simulated and observed snow depths, suggesting that uncertainties in the canopy process representations prevail in these simulations.

3.3.2 Impact of vegetation representation on soil temperature

Similar to the snow depth, soil temperature predictions by ISBA-VS are erroneous, with drastically underestimated temperatures and unrealistic dynamics (Fig. 10) (see more soil depths in Fig. S3). While MEB and ISBA-FS provided very similar snow depth, the soil temperatures simulated by MEB agree better with the observations although there is a cold bias in autumn and a warm bias in summer (Fig. 10). On N-FOR the warm bias in winter by MEB may be important for determining the soil frost regime. Interestingly, ISBA-FS seems to capture the winter soil temperatures better on N-FOR, but this may be due to the larger cold bias in autumn likely caused by the lack of explicit litter and canopy layers. All model versions tend to overestimate day-to-day temperature variability.

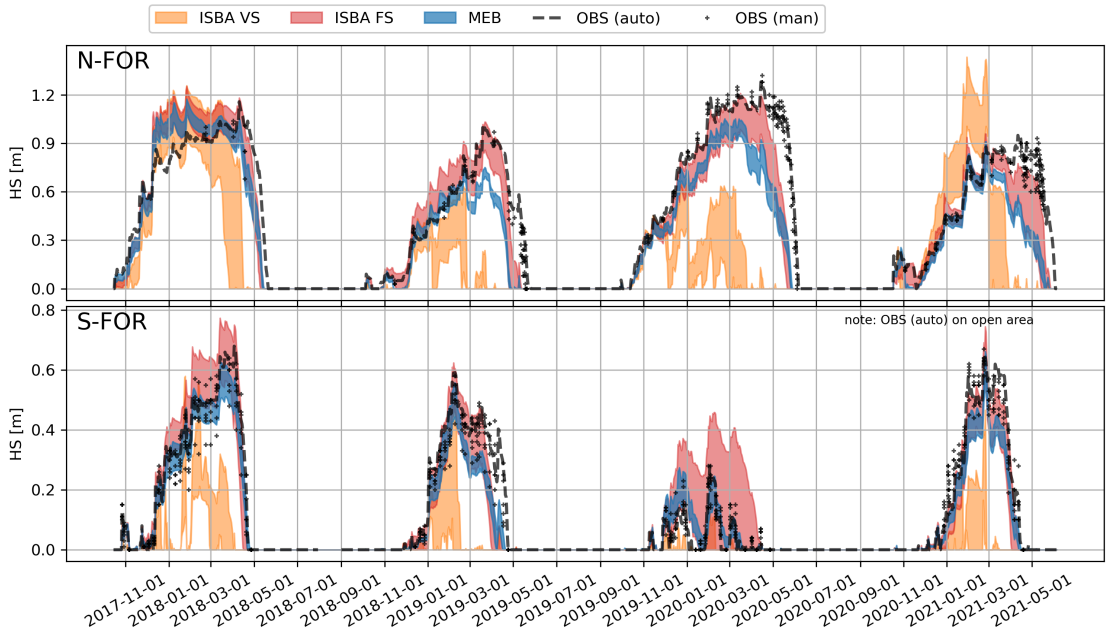

Figure 9. Effect of alternative configurations of ISBA and MEB on the snow depth (HS). The envelopes visualize the corresponding ensemble spreads between minimum and maximum values.

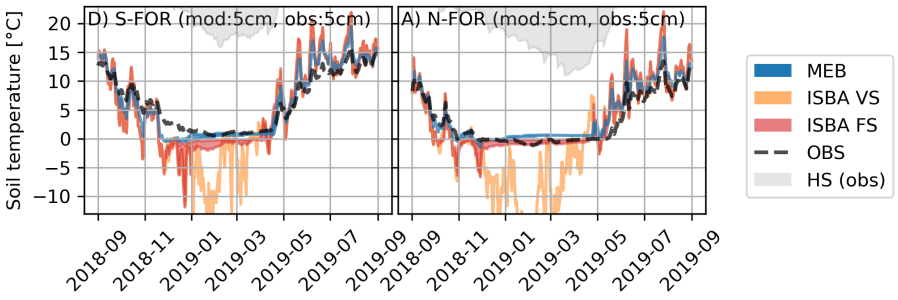

Figure 10. Effect of alternative configurations of ISBA and MEB on soil temperatures. The envelopes visualize the corresponding ensemble spreads. The observed evolution of the snow depth (HS) is not in scale. The observed soil temperatures are compared to the closest model layer; the depths of measurements and simulations are presented in each panel.

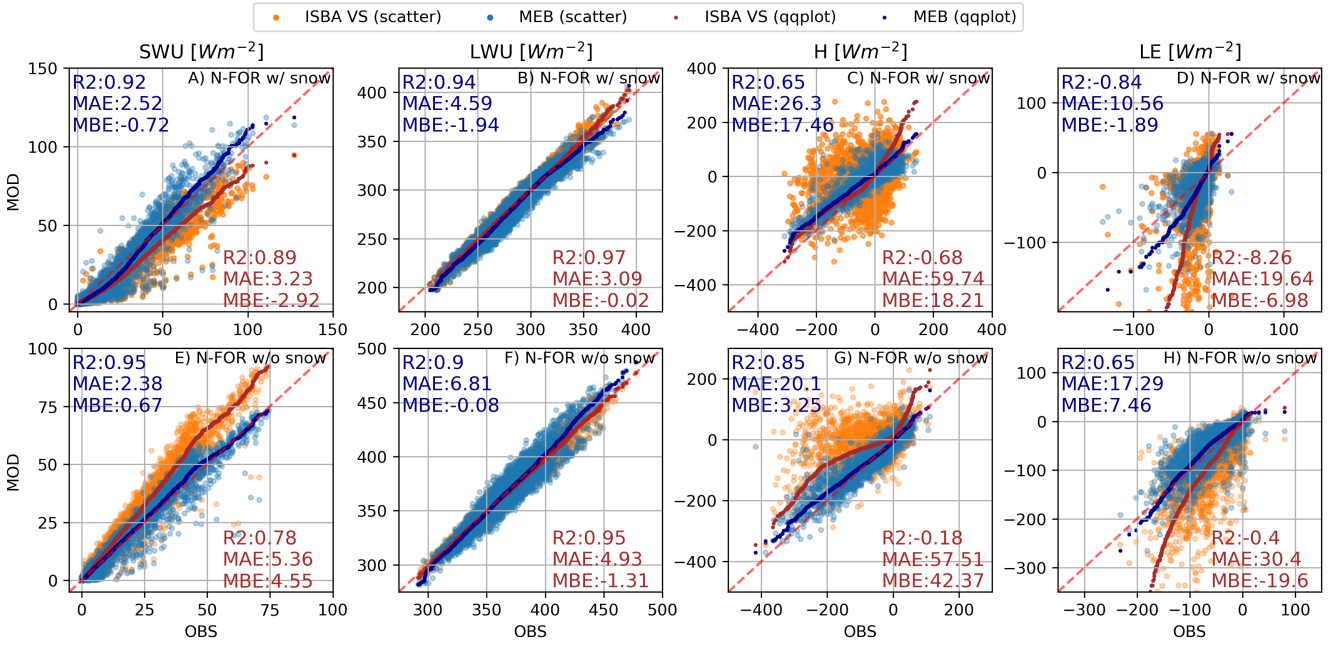

Figure 11. Simulated against observed upward short and longwave radiation (SWU and LWU, columns 1 and 2) and turbulent fluxes (H and LE, columns 3 and 4) on N-FOR site for the full evaluation period. Ground conditions are presented as i) with snow cover (w/ snow, row 1) and ii) without snow cover (w/o snow, row 2).

3.3.3 Impact of vegetation representation on surface energy fluxes

Figure 11 compares the deterministic simulations (Sect. 2.5) by MEB and ISBA-VS against observed above-canopy energy fluxes at N-FOR. The snow cover periods are defined according to agreement between MEB simulations and observations, and thus, the ISBA-VS simulations are often snow-free as seen in Fig. 9.

460 MEB is superior to ISBA-VS in simulating energy fluxes. SWU simulations with snow cover are clearly improved by MEB, but the spread remains relatively large and albedo is underestimated when incoming radiation is small and overestimated when incoming shortwave radiation is higher. The time evolution of albedo on N-FOR and S-FOR is presented in Sect 3.3.4. The LWU is very well simulated by both model configurations. Turbulent fluxes are clearly better simulated by MEB, but the performance metrics of turbulent fluxes are worse than for radiative fluxes. ISBA-VS uses vegetation fraction parameter to 465 scale the partitioning of latent heat flux between vegetation and soil (Eq. 4). However, because same roughness length and thus turbulent exchange coefficient (C_H) is used for both soil and vegetation, the soil evaporation and snow sublimation are likely overestimated and result in clearly wrong partitioning between H and LE (Fig. 11C,D and G,H). In the case of N-FOR, especially the summer energy fluxes were majorly improved by simply assigning the vegetation fraction to unity (i.e. full vegetation coverage and no soil evaporation, see Fig. S7).

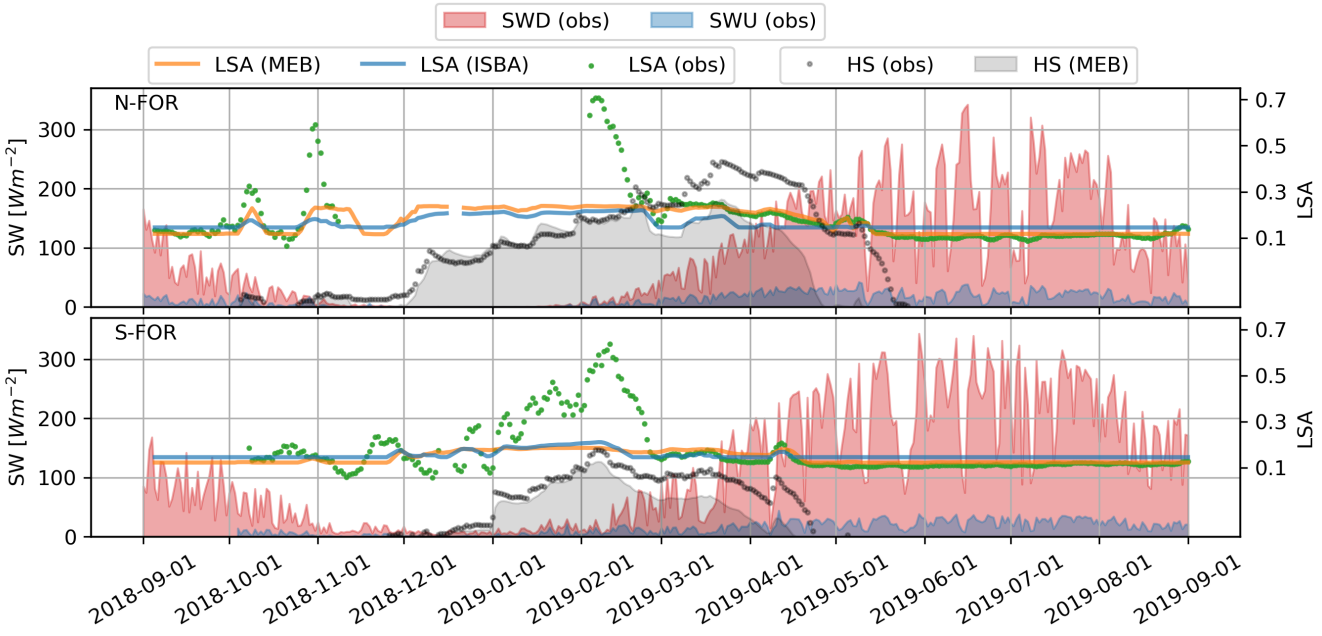

Figure 12. Simulated and observed albedo (LSA) and downward and upward shortwave radiation (SWD and SWU) in 2018–2019. LSA is presented as 5-day rolling means. The observed evolution of the snow depth (HS) is not in scale.

3.3.4 Evolution of albedo

Figure 12 illustrates the time evolution of modelled and observed albedo and the shortwave components in 2018–2019 on both forest sites. Compared to the measurements, the modelled early and mid winter albedos are underestimated while the spring albedos are slightly overestimated, consistent with results in Sect 3.3.3. The likely reason for winter albedo underestimation is because the models do not represent changes in albedo due to intercepted snow. The overestimation in spring is presumably due to representing effective albedo of snow and forest canopy with only bulk canopy parameters, as well as effect of spring needle and litter fall decreasing snow albedo. Moreover, the simulated albedo is dominated by the vegetation albedo parameter, and thus, it is not highly sensitive to snowpack albedo dynamics.

3.4 Summary: Surface energy budget on peatland and forest sites

Finally, to sum up the whole surface energy budget, we compare how the simulated R_n and turbulent fluxes (H+LE) match the observations at the four sites. These deterministic simulations are conducted with simulation setups that provided the best fit to data: the deterministic simulation as M98-SOC for the peatland sites, and deterministic MEB simulation for the forest sites (Fig. 13).

Despite the challenges in simulating snow depth evolution at the forest sites, the energy budget simulations are generally better than on the peatlands. Due to the challenges to accurately simulate albedo and surface temperatures on the open sites, the

Table 3. Occurrence of different turbulence regimes at S-WET and N-WET. The regimes are defined based on the bulk Richardson number (Ri). Unstable conditions as Ri < 0, weakly stable conditions as $0 \leq \text{Ri} \leq 0.25$, and strongly stable conditions as Ri > 0.25.

		Turbulence regimes		
Site	Surface	Unstable [%]	Weakly stable [%]	Stable [%]
N-WET	all	35.1	15.1	49.8
N-WET	snow	13.3	16.5	70.2
N-WET	ground	63.2	15.0	21.8
S-WET	all	59.7	33.7	6.6
S-WET	snow	26.5	54.6	18.8
S-WET	ground	78.9	20.5	0.6

simulated R_n is considerably worse on peatland sites than on forests (see Fig. 7). Especially the high R_n periods, representing the spring conditions, are biased on peatland sites, while the negative R_n (i.e. the winter conditions) are simulated rather well. The challenges in describing forest wintertime albedo and thus SWU (as in Fig. 12 and Fig. 11) do not significantly bias the R_n simulations, as in wintertime the shortwave radiation balance has small role compared to the longwave radiation balance. The results propose that canopy temperature, which particularly in dense forests (e.g. S-FOR) has central role for upward longwave radiation, must be adequately simulated by MEB. When it comes to the turbulent fluxes, the simulations capture the main seasonal patterns. However, there are still high uncertainties (scatter) both on peatland and forest sites. The relative uncertainties in simulated and observed energy fluxes are significantly greater in winter than in summer. Performance of the simulated summer energy fluxes is very good (Fig. S4).

4 Discussion

4.1 Insights on energy flux partitioning in boreal environments

The energy budget observed with this novel dataset over boreal and subarctic peatlands showed that despite the prevailing stable atmospheric conditions (Table 3), the radiative cooling was mostly counterbalanced by sensible heat flux (H) (Fig. 3). During the snow season, the dominating regimes were strongly stable at N-WET (70.2 %) and weakly stable at S-WET (54.6 %). Despite the stronger stability at N-WET, we observed higher H fluxes compared to S-WET, and considerably higher H than Lackner et al. (2021) at the Canadian site dominated by weakly stable conditions. Thus, we presume that greater radiative cooling leads to stronger near-surface air temperature gradient and larger downward sensible heat flux.

The small role of the ground heat flux (G) at the studied peatlands is due to the high heat capacity of the peat soil, and its large water storage which progressively freezes from the top keeping the temperatures in the soil-snow interface nearly constant at minimum 0°C (Fig. 8). Other studies in tundra environments of the Canadian Arctic, Siberia and Svalbard have reported larger contributions of G to the wintertime energy budget (Lackner et al., 2021; Langer et al., 2011; Westermann et al., 2009).

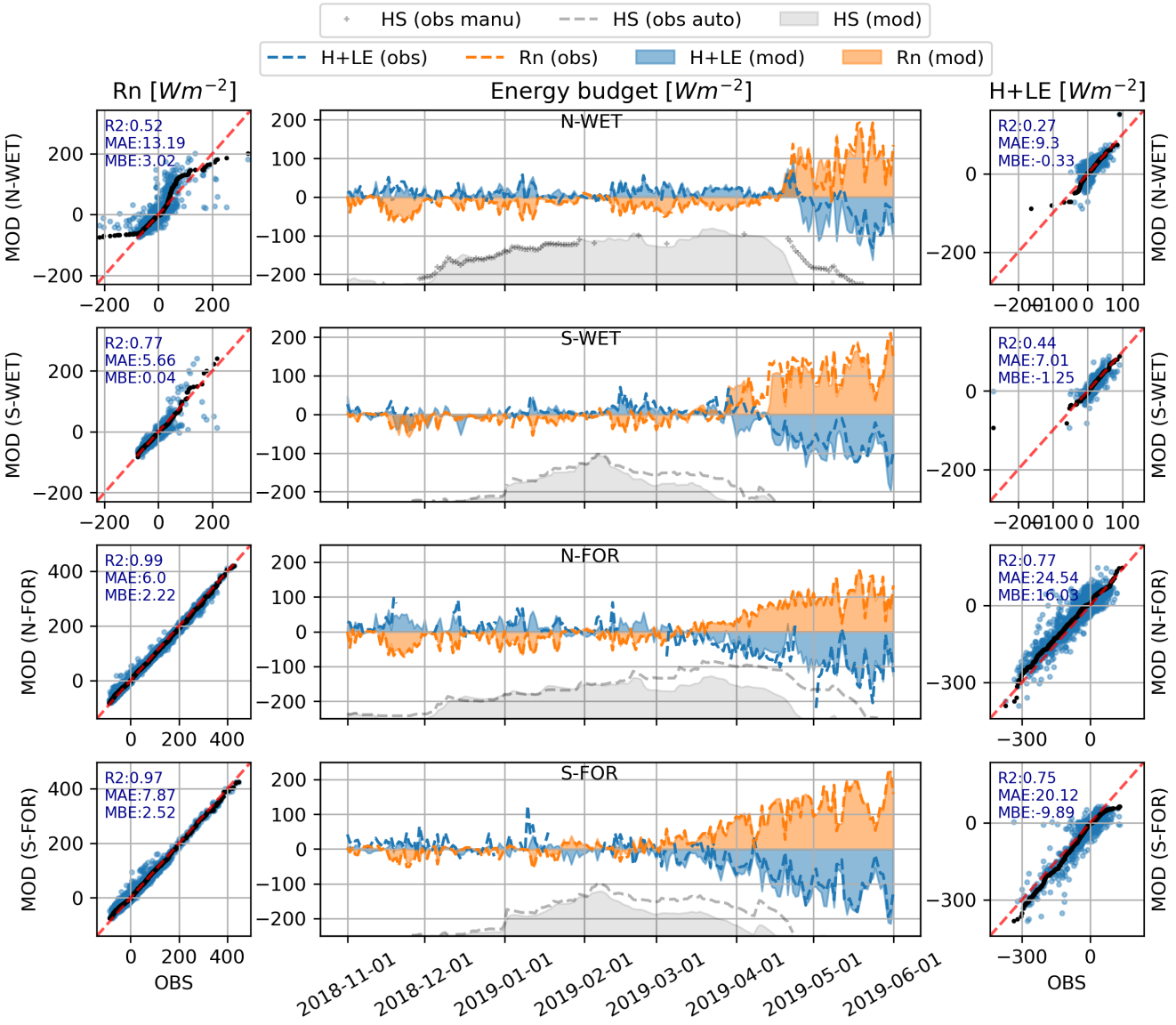

Figure 13. Simulated (MOD) against observed (OBS) daily surface energy budget during winter 2018-2019. The left column shows net radiation (R_n) and right column presents the sum of turbulent fluxes (H+LE). The scatter plots represent full simulation periods when snow cover was present. The observed evolution of the snow depth (HS) is not in scale.

We observed shorter snow melt period in the peatlands compared to adjacent forest sites (see Fig. S5), in line with Lundquist et al. (2013), who proposed that increased canopy shading (delaying melt) outweighs the impact of longwave radiation enhancement (accelerating melt). Our datasets support this (Fig. S5); however, the forest sites tended to also accumulate more snow than the peatland sites (wind erosion is presumably higher on peatlands), which may have contributed to longer snow duration in the forest.

4.2 Implications for simulating snow and energy balance at peatland sites

Our results highlighted the uncertainties in modelling turbulent fluxes over snowpack, and identified the turbulent exchange parameterizations (M98-SOC and RI2-SOC) that improve the simulated surface energy fluxes and snowpack dynamics at high-latitude winter conditions (Fig. 5, 6). In stable (winter) conditions, the uncertainties in turbulent fluxes are in line with Menard et al. (2021); Conway et al. (2018); Lapo et al. (2019), and larger than in unstable (summer) conditions (Fig. S4). Moreover, the turbulent fluxes of sensible and latent heat have greater uncertainty than the radiation balance components (Fig. 13). The ESCROC-E_2 simulations showed that the turbulent exchange parameterizations have also impact on snow melt simulations, in line with simulations at Col de Porte, France and ESM-SnowMIP sites (Menard et al., 2021). In contrast, Lackner et al. (2021) found only small differences between the Crocus turbulence parameterizations in their study in the Canadian Arctic, most likely due to smaller sensible heat fluxes and less frequent strongly stable conditions.

Improved surface temperature simulations by the M98-SOC (absolute biases decreased by 0.3 °C at S-WET and 0.4 °C at N-WET compared to RIL-SOC) provide support to Martin and Lejeune (1998) and Gouttevin et al. (2023), who adjusted the turbulent fluxes under stable conditions to reproduce surface and air temperature observations. The default ISBA turbulent flux parameterization (RIL), although widely used e.g. in numerical weather prediction and general circulation models (Mahfouf et al., 1995; Salas-Mélia et al., 2005; Voldoire et al., 2013, 2019), provided the poorest fit with the observed surface heat fluxes, and produced a cold bias in snow surface temperature (-0.4°C at S-WET and -1.1°C at N-WET). This finding is consistent with ESM-SnowMIP (Menard et al., 2021), where the default configuration of Crocus had one of the lowest skill for surface temperature simulations (-2°C mean cold bias) among the compared snow models. Even with the M98-SOC simulation we found rather low skill of turbulent flux simulations. To summarize, our findings highlight the limitations of the Monin-Obukhov similarity theory to simulate turbulent fluxes under stable atmospheric conditions, and emphasize the need for further model developments with observations in various environments.

The soil temperature simulations confirmed that it is necessary to realistically describe the organic peat soil hydraulic and thermal properties (Menberu et al., 2021; Morris et al., 2022; Mustamo et al., 2019) to accurately simulate soil thermal regime and consequent freezing/thawing processes in peatlands (Fig. 8) (Dankers et al., 2011; Lawrence and Slater, 2008; Nicolsky et al., 2007). This is line with Decharme et al. (2016) who implemented SOC parameterization in ISBA, and showed improved soil temperature simulations across northern Eurasia. Implementation of water table dynamics and lateral flow could further improve the soil temperature simulations on boreal and subarctic peatlands. The thermal state and ice/liquid water content have also major cascading effects on runoff generation during snow melt (Ala-Aho et al., 2021). Moreover, the interactions between low vegetation and snow are likely improved by using explicit vegetation (MEB in SURFEX). However, as MEB

has never been applied on snow-covered low vegetation, additional development and evaluation would have been required that were beyond the scope of this study.

4.3 Implications for simulations at forest sites

4.3.1 ISBA-VS

We found the ISBA-VS to be largely biased towards correctly simulated surface energy fluxes at the expense of poor soil temperature and snow depth simulations, as a major part of the composite was always directly coupled to the atmosphere (Fig. 9, 10). ISBA-VS with correct tuning (e.g. setting veg. fraction to unity on N-FOR), may be an imperfect but sufficient compromise to simulate snow-free forests in applications that first and foremost require grid-cell averaged surface energy fluxes (i.e. numerical weather prediction). However, we agree with Napoly et al. (2020) that the snow cover fraction approach of ISBA (Fig. 2B) is essentially a compromise that attempts to retain the insulating impact of the snowpack over the soil while still simulating turbulent exchange from the vegetation. The energy exchange between the atmosphere and the soil-vegetation composite directly impacts the snowpack, and led to strongly biased snow depth simulations, similar to Napoly et al. (2020). This fractional approach and high sensitivity of empirically based parameters (e.g. veg. fraction) highlights the uncertainties of ISBA-VS to provide accurate year-around lower boundary conditions of boreal forests for numerical weather prediction and general circulation model applications. Also considering the very low skill obtained in snow depth and soil temperatures for this configuration, its use in hydrological applications or surface offline reanalyses (Le Moigne et al., 2020) is highly questionable. Nevertheless, local-scale evaluation might not directly translate to large-scale spatial simulations, as further discussed in Sect. 4.4.

4.3.2 ISBA-FS

We found that snow and soil simulations in forests were strongly improved when the snow cover fraction was set to unity (ISBA-FS), allowing the snowpack to fully insulate the soil, similarly to the simulations at the peatland sites (Fig. 9). These results suggest that if the focus is on snowpack dynamics and soil temperature simulations, ignoring snow-vegetation interactions is a better compromise than using varying snow cover fraction as it is currently implemented in SURFEX. Consequently, ISBA-FS should be preferred to ISBA-VS in surface reanalyses as in Brun et al. (2013); Vernay et al. (2022). However, ISBA-FS reaches its conceptual limits when forest energy balance, snow, and soil state variables are all of interest. For instance, neglecting snow interception and subsequent canopy snow losses may cause large errors in simulated snow water equivalent in dense forests, and unrealistic contribution of the canopy evapotranspiration may be expected if reanalyses are further used for hydrological modelling. Obviously, highly biased surface energy fluxes would also be expected for any coupling with an atmospheric model.

4.3.3 MEB

MEB appears as a better compromise than ISBA-VS and ISBA-FS for modelling forest energy exchanges; the snow depth and soil temperature simulations were highly improved compared to ISBA-VS while surface-atmosphere energy fluxes are obviously much more realistic than with ISBA-FS. Significant improvements in energy flux simulations were also obtained compared to ISBA-VS (Fig. 11).

Nevertheless, two systematic biases affecting upward shortwave radiation were identified: albedo was underestimated in winter and overestimated in spring (Fig. 12). The winter albedo underestimation was most likely because intercepted snow increased the observed albedo, a process that is not accounted for in MEB (Napoly et al., 2020). This assumption is based on Pomeroy and Dion (1996), while the increase of forest albedo by intercepted snow has been more recently shown (Webster and Jonas, 2018), and simple descriptions can already be found in some forest snow models (Mazzotti et al., 2020a). Although our results propose that the intercepted snow has a clear impact on the albedo, its impact on R_n was small. The spring albedo bias is in line with Malle et al. (2021), who found albedo at sparse boreal forests to be overestimated by the LSM CLM5. Big-leaf canopy parameterizations may fail to fully capture canopy shading, particularly at low solar elevation angles typical of high latitudes (Malle et al., 2021).

In contrast to Napoly et al. (2020), we found MEB to systematically simulate too early snow melt, especially on N-FOR (Fig. 9). These errors are partly explained by inaccuracies in canopy radiative transfer, but they also suggest errors in simulated below-canopy surface heat fluxes. The differences in snow simulations were rather small between MEB and ISBA-FS especially at N-FOR, suggesting that sparse canopies did not majorly alter simulated snow accumulation and ablation, at least when compared to snow depth observations between the trees. Consistently, Meriö et al. (2023) have shown decreased snow depths at the immediate vicinity of tree trunks, but high snow depth between trees at N-FOR.

4.4 Limitations and outlook

Our eddy-covariance fluxes are among the longest datasets ever used for the evaluation of turbulent flux simulations over snow. The EC-data, however, contains both random and systematic uncertainties (e.g. Aubinet et al., 2012). The absolute values of winter H and LE are small and their relative uncertainty is high; compared to summertime measurements the wintertime energy balance closure ratio is typically poorer particularly at the northern ecosystems (Reba et al., 2009; Molotch et al., 2009; Launiainen, 2010). As our analysis used numerous site years from multiple sites, and we used established quality criteria for filtering the EC-fluxes, we expect that uncertainties in flux data do not significantly affect the study results. Moreover, the conclusions regarding the validity of each model version were not affected by selected flux quality flag (Sect. 2.4.2). Intrinsic uncertainties in meteorological forcing are known to exist, especially in northern conditions (instrument freezing, snow blocking, undercatch etc., Stuefer et al., 2020), and data gaps further add up possible sources of errors. Uncertainties in model forcing can affect model-data comparisons, especially during the gap-filled periods (Raleigh et al., 2015).

Potentially important snow processes on subarctic sites are still absent in Crocus, including wind-induced snow transport and internal water vapor transfer due to large temperature gradient in the snowpack. Wind can move and change the properties of snow (Pomeroy and Essery, 1999; Meriö et al., 2023; Liston and Sturm, 2002), and is especially noticeable on open peatlands. In Crocus, wind modifies the properties of falling snow (Vionnet et al., 2012) but without any lateral transport or modifications of the mass. Although we achieved satisfactory model performance without accounting for this process, Meriö et al. (2023) showed notable wind transport in transition zones between open peatland and forest at the N-WET site. Although the spatial scale of wind transport prevents an explicit simulation of this process in large-scale LSMs, improved parameterizations of the wind impact on snow properties should be considered in the future. Omission of internal water vapor transfer by diffusion and/or convection has been suspected to be responsible for errors in simulated snow properties (density, microstructure) in Arctic snowpack (Barrere et al., 2017; Domine et al., 2018) and consequently in thermal conductivity and soil thermal regime. A realistic implementation of water vapor transfer within the snowpack is lacking in most state-of-the-art LSMs. Complementary observations and model developments are required to understand if the simulated snow properties are affected by this kind of errors. Furthermore, the spring and autumn conditions on the peatlands are particularly difficult to correctly simulate; in addition to the snow cover, also e.g. ponding of liquid water and refreezing of the ponds are not uncommon (Noor et al., 2022) and can alter the albedo.

In forests, the spatial heterogeneity of snow cover can be high, as demonstrated by numerous studies (Marttila et al., 2021; Mazzotti et al., 2020b; Noor et al., 2022) and confirmed by our data (Fig. 9). The small-scale forest structure has an important role in the evolution of the snow cover, and may affect the representativeness of point measurements (Bouchard et al., 2022). Consequently, the comparison of point observations and models intended for forest stand and larger scales (such as the big-leaf approach of MEB), can suffer from this scale miss-match (Essery et al., 2009; Rutter et al., 2009). More realistic below and above canopy heat flux simulation could be achieved by more sophisticated canopy representations, including multiple layers and species (Bonan et al., 2021; McGowan et al., 2017; Launiainen et al., 2015; Gouttevin et al., 2015). For site-level or limited area modelling, high resolution models that explicitly resolve tree-scale canopy structure are a promising alternative to traditional LSMs (Broxton et al., 2015; Mazzotti et al., 2020b).

The generality of our findings should be tested by additional snow model and LSM evaluation studies, extended to more contrasting climates and wider range of ecosystem types. For this purpose, model evaluation datasets should be complemented with more boreal and Arctic sites and observations of all components of surface energy balance, particularly turbulent fluxes.

5 Conclusions

We used eddy-covariance based energy flux data, radiation balance and snow depth and soil temperature measurements in two boreal and subarctic peatlands and forests to evaluate turbulent exchange parameterizations and alternative approaches to represent the soil and vegetation continuum in land surface models. We used the SURFEX platform but our findings are largely transferable to other model systems. Our evaluation with the ensemble snowpack parameterizations (ESCROC-E_2) ensures that uncertainties in snow processes (not evaluated in this study) do not affect the robustness of our main conclusions.

Peatland simulations showed that using a stability correction function that increases the turbulent exchange under stable atmospheric conditions is imperative to simulate the snowpack energy budget. This adjustment led to major improvements under stable conditions during snow cover, but the model performance still remained lower than in snow-free conditions. Furthermore, correct hydraulic and thermal parameterization of organic peat soils was found necessary to reproduce the observed soil thermal regime in peatlands. The findings have direct implications for modelling snow dynamics, peatland hydrology as well as permafrost dynamics.

The surface energy budgets of forest sites were well simulated by the explicit big-leaf approach (MEB), while the composite soil-vegetation approach (ISBA-VS) performance was satisfactory only after an adjustment of a sensitive vegetation fraction parameter. In particular, shortwave and longwave radiation balances were simulated well by both approaches, whereas the turbulent fluxes had significantly higher uncertainty. Only the explicit vegetation model (MEB) was able to simultaneously simulate realistic surface energy budget and snow/soil conditions. The composite approaches only succeeded in either simulating the correct surface energy budget (ISBA-VS) or snow/soil conditions (ISBA-FS). Furthermore, we demonstrated that the composite approaches rely on a previously poorly documented parameterization of the snow cover fraction with high sensitivity on model outputs despite a limited physical interpretation.

With well-selected model configuration and parameterization, SURFEX model platform can realistically simulate surface energy fluxes and snow and soil conditions in the subarctic and boreal peatlands and forests. The common version of ISBA (ISBA-VS) can provide rather realistic lower boundary conditions for numerical weather prediction and global circulation models, at the expense of non-realistic predictions of forest snow and soil conditions necessary for hydrological applications. We expect that the future inclusion of MEB in operational systems will reconcile these applications. Our results can be used to inform the choice of model configuration for studies of subarctic and boreal regions ecology, hydrology and biogeochemistry under the ongoing environmental change.

Author contributions.

JPN, ML, SL, PA and HM designed the research. JPN led the study and was in charge of the experiments. JPN, GM and ML performed the model evaluations with scientific contributions of SL, HM and PA. JPN was responsible for writing the article, with significant contributions from GM, ML and SL and input from all the authors. BC and MF supported the ensemble simulations and other technical aspects. MA, AL, PK, PA and HM provided surface energy data and ancillary data.

Competing interests.

The authors declare that they have no conflict of interest.

Acknowledgements. This work was funded by the Research Council of Finland (RCF) (ArcI Profi 4). GM was funded by the Swiss National Science Foundation (Grant P500PN_202741). SL and JPN acknowledges GreenFeedBack project from the EU Horizon Europe – Framework Programme for Research and Innovation (no. 101056921). SL thanks the support of RCF (LS-HYDRO, 356138). PA was funded by the RCF Research Fellow grant (no. 347348). PK, MA and AL thank the support from the ACCC Flagship funded by the RCF (no. 337549 and no. 337552) and ICOS-Finland by University of Helsinki and the Ministry of Transport and Communication. MA and AL also acknowledge the RCF (UPFORMET, grant no. 308511). JPN thanks Riitta ja Jorma Takasen säätiö for internationalization support grant. The authors would like to thank Bertrand Decharme, Christine Delire, Bertrand Bonan at CNRM/GAME and Marie Dumont at CNRM/CEN for their great support during this work. CNRM/CEN is part of Labex OSUG@2020.

Code availability.

The SURFEX is an open source project (http://www.umr-cnrm.fr/surfex) but it requires registration. The full procedure and instructions are available at https://opensource.umr-cnrm.fr/projects/snowtools_git/wiki/Procedure_for_new_users. The SURFEX version used in this work is available in git (tagged as *boreal_ecosystems*). The ESCROC version developed for external SURFEX users, is available at https://github.com/bertrandcz/CrocO_toolbox.

Data availability.

Meteorological data, evaluation data and SURFEX specific namelist and forcing files are available as an electronic supplement at https://doi.org/10.5281/zenodo.8252267 under the terms and conditions of the Creative Commons Attribution 4.0 International license

Appendix A: Tables of abbreviations, acronyms and mathematical symbols

Table A1. Table of acronyms and abbreviations.

Acronyms and abbreviations	Definition
LSM	Land surface model
LSA	Land surface albedo
LAI	Leaf area index
LWD	Downward longwave radiation
LWU	Upward longwave radiation
SWD	Downward shortwave radiation
SWU	Upward shortwave radiation
H	Sensible heat
LE	Latent heat
R_n	Net radiation
G	Snowpack-ground heat flux
SOC	Soil organic content
EC	Eddy-covariance
HS	Snow depth
RIL	Classical Louis (1979) formula for the turbulent exchange coefficient
RI1	RIL with threshold at R_i = 0.1
RI2	RIL with threshold at R_i = 0.026
M98	Martin and Lejeune (1998) formula for C_H
BOGR	Boreal grass
BONE	Boreal needleleaf evergreen
FMI	Finnish Meteorological Institute
SMEAR	Station for Measuring Forest Ecosystem–Atmosphere Relations
FST	Flux stationarity

Table A2. Table of mathematical symbols (Part I).

Symbol	Definition
ϵ	surface emissivity
σ	Stefan-Boltzman constant
T_s	surface temperature
ρ_a	air density
ρ_w	liquid water density
ρ	snow density
c_p	specific heat capacity
V_a	wind speed
T_a	air temperature
C_H	turbulent exchange coefficient
ET	total evapotranspiration
E_g	evaporation from the bare soil surface
E_c	evaporation of intercepted water on the canopy
E_{tr}	transpiration from the vegetation
S_i	sublimation from bare soil ice
L_v	latent heat of vaporization
L_f	latent heat of fusion
veg	fraction of vegetation cover
$q_{sat}(T_s)$	saturated specific humidity at the surface
$q_a(T_s)$	atmospheric specific humidity
h_u	dimensionless relative humidity at the ground surface related to the superficial soil moisture content
h_v	dimensionless Halstead coefficient describing the Ec and Etr partitioning between the leaves covered and not covered by interc
z_u	reference height of the wind speed
z_a	reference height of the air temperature and humidity
z_{0t}	roughness height for heat
k	von Karman constant
R_i	bulk Richardson number

Table A3. Table of mathematical symbols (Part II).

Symbol	Definition
C_v	effective heat capacity of the canopy
$C_{g,1}$	effective heat capacity of the ground surface/litter layer (uppermost layer)
$C_{n,1}$	effective heat capacity of the snowpack (base layer)
T_v	temperature of the canopy
$T_{g,1}$	temperature of the ground surface/litter layer (uppermost layer)
$T_{n,1}$	temperature of the snowpack (base layer)
R_{nv}	net radiation of the canopy
R_{ng}	net radiation of the ground surface/litter layer
R_{nn}	net radiation of the snowpack
k	snow effective thermal conductivity
LE_s	latent heat flux of the snowpack
G_n	heat conduction at the snow-soil interface
p_{sn}	effective snow cover fraction
p_{snv}	effective snow cover fraction of the vegetation
p_{sng}	effective snow cover fraction of the soil
HS_g	threshold value for height of the snow
w_{sw}	coefficient relating to vegetation characteristics
E_2	ESCROC optimized standard subensemble
P	precipitation rate
P_{ice}	snowfall rate
P_{liq}	rainfall rate
r	diffuse to total shortwave radiation ratio
μ	cosine of the sun zenith angle
u_*	friction velocity

Appendix B: Model evaluation data availability and radiation forcing evaluation

The availability periods of the model evaluation data are presented in B1.

Table B1. Model evaluation data availability for each site.

Variable	N-WET	S-WET	N-FOR	S-FOR
Snow depth	2017-11–2021-05	2016-09–2021-07	2013-09–2020-09	2008-09–2021-07
Soil temperature	2013-09–2019-12	2017-06–2021-07	2016-09–2020-09	2008-09–2021-07
Upward LW flux	2017-07–2021-06	2016-09–2021-07	2013-09–2021-07	2008-09–2021-07
Upward SW flux	2017-07–2021-06	2016-09–2021-07	2013-09–2021-07	2008-09–2021-07
Sensible heat flux	2013-09–2021-06	2016-09–2020-12	2013-09–2021-07	2008-09–2021-07
Latent heat flux	2013-09–2021-06	2016-09–2020-12	2013-09–2021-07	2008-09–2021-07
Ground heat flux	2013-09–2017-07	2016-09–2021-07	2013-09–2021-02	2008-09–2021-07

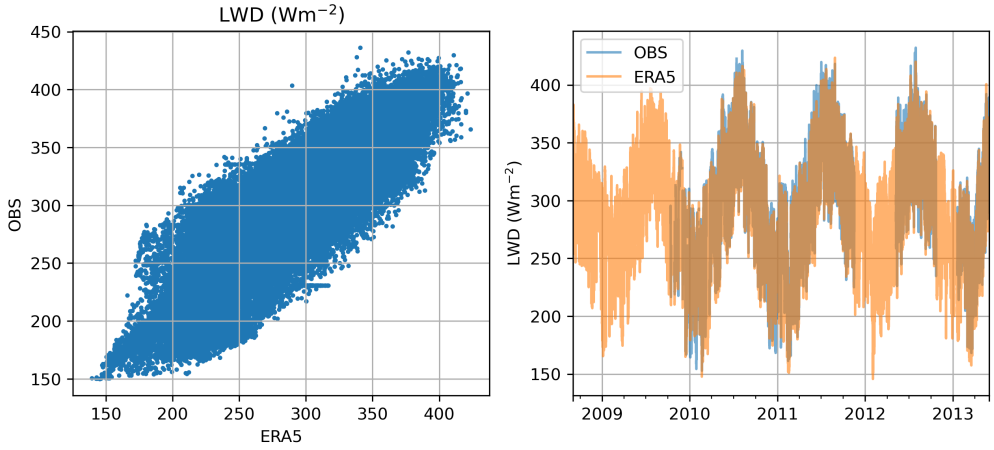

Figure B1. Comparison of longwave radiation forcing data between ERA5 and site observations (OBS) on S-FOR.

Appendix C: Effect of snow cover fraction parameter w_{sw}

Table C1. Summary of snow cover fraction and values of w_{sw} used in different SURFEX/ISBA applications. The parameter w_{sw} is rarely documented, and hence, these application specific values were obtained through communications with the authors.

Application	Name	Domain	Resolution	Snow fraction	w_{sw}	Reference
Numerical weather prediction	AROME, ARPEGE	Europe (many)	1.3 - 10 km	varying	5	Bengtsson et al. Courtier et al. (1
Global climate modelling	CNRM-CM6	Global	100 km	varying	2	Decharme et al.
Regional climate modelling	CNRM-AROME	European Alps	2.5 km	varying	1	Caillaud et al. (2
Regional climate modelling	CNRM-ALADIN	Europe, North Africa	12 km	varying	2	Nabat et al. (202
Hydrological modelling	SIM2	France	8 km	varying	0.2	Le Moigne et al.
Regional reanalysis	CERRA-Land	Europe	5.5 km	varying	0.1	Verrelle et al. (20
Snow cover reanalysis	S2M	French Alps	massif-scale	full (1)	-	Vernay et al. (20
Snow cover reanalysis	ERA-Interim-Crocus	Northern Eurasia	80 km	full (1)	-	Brun et al. (2013
Avalanche hazard forecasting	S2M	French Alps	massif-scale	full (1)	-	Morin et al. (202

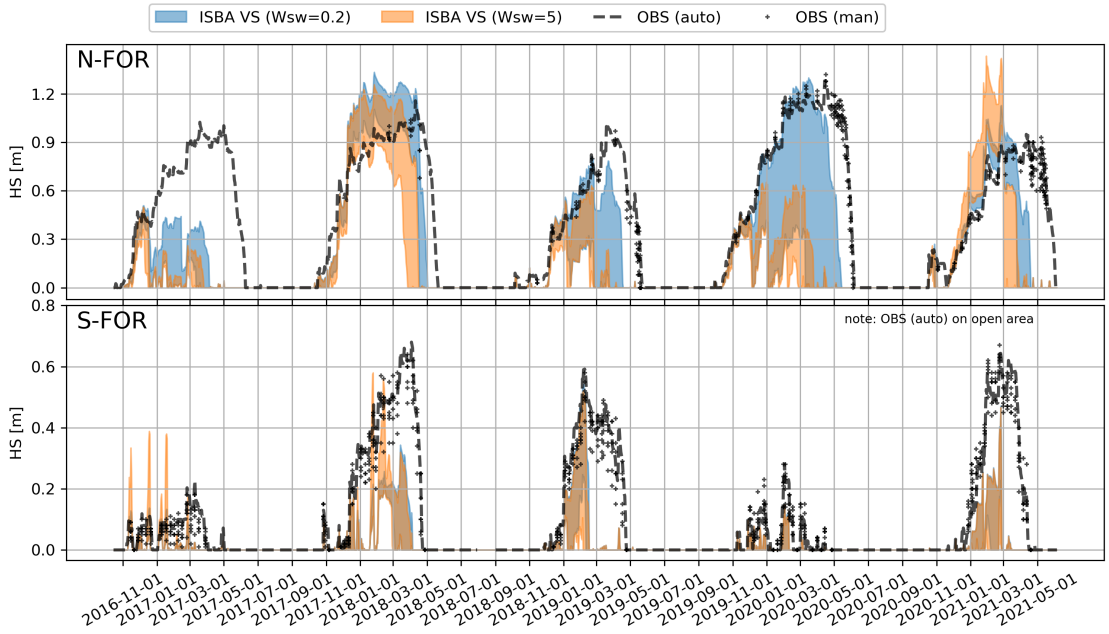

Figure C1. Effect of w_{sw} parameter on snow depths simulated by ISBA-VS. The envelopes visualize the corresponding ensemble spreads between minimum and maximum values.

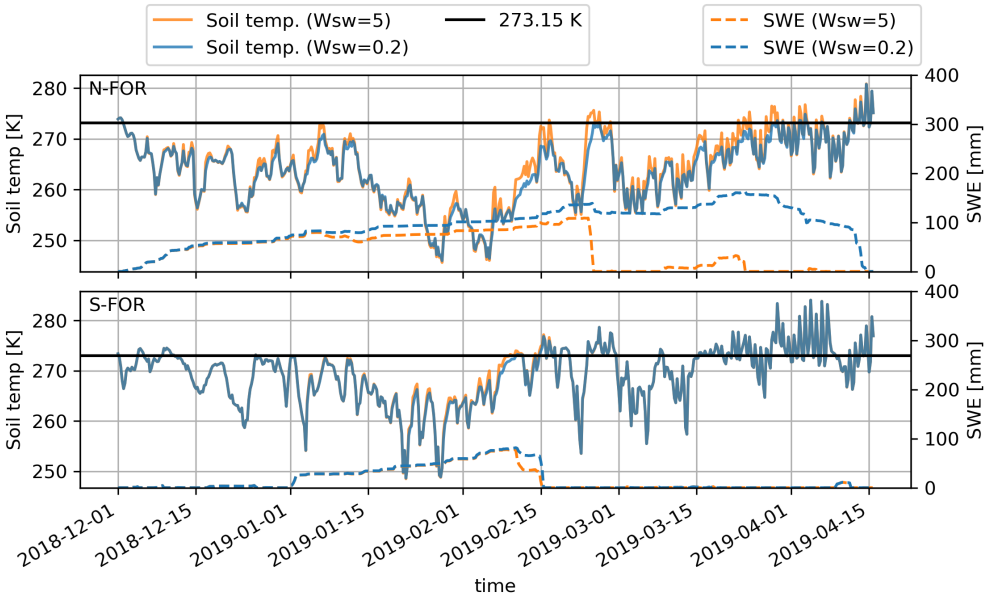

Figure C2. The sensitivity of w_{sw} parameter on 6-hour surface soil temperature simulations and snow water equivalent (SWE). Simulations are represented by one member of the ESCROC-E_2 ISBA VS.

References

Aalto, J., Aalto, P., Keronen, P., Kolari, P., Rantala, P., Taipale, R., Kajos, M., Patokoski, J., Rinne, J., Ruuskanen, T., and others: SMEAR II Hyytiälä forest meteorology, greenhouse gases, air quality and soil, \url{https://doi.org/10.23729/62f7ad2c-7fe0-4f66-b0a4-8d57c80524ec}, 2022.

Ala-Aho, P., Autio, A., Bhattacharjee, J., Isokangas, E., Kujala, K., Marttila, H., Menberu, M., Meriö, L. J., Postila, H., Rauhala, A., Ronkanen, A. K., Rossi, P. M., Saari, M., Haghighi, A. T., and Klove, B.: What conditions favor the influence of seasonally frozen ground on hydrological partitioning? A systematic review, Environmental Research Letters, 16, https://doi.org/10.1088/1748-9326/abe82c, 2021.

Alekseychik, P., Kolari, P., Rinne, J., Haapanala, S., Laakso, H., Taipale, R., Matilainen, T., Salminen, T., Levula, J., Tuittila, E.-S., and others: SMEAR II Siikaneva 1 wetland meteorology and soil, \url{https://doi.org/10.23729/7d205559-3ef9-4f34-8e08-ea24316f50c8}, 2022a.

Alekseychik, P., Peltola, O., Li, X., Aurela, M., Hatakka, J., Pihlatie, M., Rinne, J., Haapanala, S., Laakso, H., Taipale, R., and others: SMEAR II Siikaneva 1 wetland eddy covariance, \url{https://doi.org/10.23729/f6455f02-905b-4bf7-a870-743bd3788bf6}, 2022b.

Alekseychik, P. K., Korrensalo, A., Mammarella, I., Vesala, T., and Tuittila, E. S.: Relationship between aerodynamic roughness length and bulk sedge leaf area index in a mixed-species boreal mire complex, Geophysical Research Letters, 44, 5836–5843, https://doi.org/10.1002/2017GL073884, 2017.

Andreas, E. L., Horst, T. W., Grachev, A. A., Persson, P. O. G., Fairall, C. W., Guest, P. S., and Jordan, R. E.: Parametrizing turbulent exchange over summer sea ice and the marginal ice zone, Quarterly Journal of the Royal Meteorological Society, 136, 927–943, https://doi.org/10.1002/qj.618, 2010.

Aubinet, M., Vesala, T., and Papale, D.: Eddy covariance: a practical guide to measurement and data analysis, Springer Science & Business Media, 2012.

Aurela, M., Riutta, T., Laurila, T., Tuovinen, J. P., Vesala, T., Tuittila, E. S., Rinne, J., Haapanala, S., and Laine, J.: CO2 exchange of a sedge fen in southern Finland - The impact of a drought period, Tellus, Series B: Chemical and Physical Meteorology, 59, 826–837, https://doi.org/10.1111/j.1600-0889.2007.00309.x, 2007.

Aurela, M., Lohila, A., Tuovinen, J. P., Hatakka, J., Penttilä, T., and Laurila, T.: Carbon dioxide and energy flux measurements in four northern-boreal ecosystems at Pallas, Boreal Environment Research, 20, 455–473, 2015.

Barrere, M., Domine, F., Decharme, B., Morin, S., Vionnet, V., and Lafaysse, M.: Evaluating the performance of coupled snow-soil models in SURFEXv8 to simulate the permafrost thermal regime at a high Arctic site, Geoscientific Model Development, 10, 3461–3479, https://doi.org/10.5194/gmd-10-3461-2017, 2017.

Bengtsson, L., Andrae, U., Aspelien, T., Batrak, Y., Calvo, J., Rooy, W. d., Gleeson, E., Hansen-Sass, B., Homleid, M., Hortal, M., Ivarsson, K. I., Lenderink, G., Niemelä, S., Nielsen, K. P., Onvlee, J., Rontu, L., Samuelsson, P., Muñoz, D. S., Subias, A., Tijm, S., Toll, V., Yang, X., and Køltzow, M. : The HARMONIE-AROME model configuration in the ALADIN-HIRLAM NWP system, Monthly Weather Review, 145, 1919–1935, https://doi.org/10.1175/MWR-D-16-0417.1, 2017.

Beringer, J., Lynch, A. H., Chapin, F. S., Mack, M., and Bonan, G. B.: The representation of arctic soils in the land surface model: The importance of mosses, Journal of Climate, 14, 3324–3335, https://doi.org/10.1175/1520-0442(2001)014<3324:TROASI>2.0.CO;2, 2001.

Blyth, E. M., Arora, V. K., Clark, D. B., Dadson, S. J., De Kauwe, M. G., Lawrence, D. M., Melton, J. R., Pongratz, J., Turton, R. H., Yoshimura, K., and Yuan, H.: Advances in Land Surface Modelling, Current Climate Change Reports, 7, 45–71, https://doi.org/10.1007/s40641-021-00171-5, 2021.

Boisvert, L. N. and Stroeve, J. C.: The Arctic is becoming warmer and wetter as revealed by the Atmospheric Infrared Sounder, Geophysical Research Letters, pp. 4439–4446, https://doi.org/10.1002/2015GL063775.Received, 2015.

Bonan, G. B., Patton, E. G., Finnigan, J. J., Baldocchi, D. D., and Harman, I. N.: Moving beyond the incorrect but useful paradigm: reevaluating big-leaf and multilayer plant canopies to model biosphere-atmosphere fluxes – a review, Agricultural and Forest Meteorology, 306, 108 435, https://doi.org/10.1016/j.agrformet.2021.108435, 2021.

Boone, A., Masson, V., Meyers, T., and Noilhan, J.: The influence of the inclusion of soil freezing on simulations by a soil-vegetation-atmosphere transfer scheme, Journal of Applied Meteorology, 39, 1544–1569, https://doi.org/10.1175/1520-0450(2000)039<1544:TIOTIO>2.0.CO;2, 2000.

Boone, A., Samuelsson, P., Gollvik, S., Napoly, A., Jarlan, L., Brun, E., and Decharme, B.: The interactions between soil-biosphere-atmosphere land surface model with a multi-energy balance (ISBA-MEB) option in SURFEXv8-Part 1: Model description, Geoscientific Model Development, 10, 843–872, https://doi.org/10.5194/gmd-10-843-2017, 2017.

Bouchard, B., Nadeau, D. F., and Domine, F.: Comparison of snowpack structure in gaps and under the canopy in a humid boreal forest, Hydrological Processes, 36, https://doi.org/10.1002/hyp.14681, 2022.

Broxton, P. D., Harpold, A. A., Biederman, J. A., Troch, P. A., Molotch, N. P., and Brooks, P. D.: Quantifying the effects of vegetation structure on snow accumulation and ablation in mixed-conifer forests, Ecohydrology, 8, 1073–1094, https://doi.org/10.1002/eco.1565, 2015.

Brun, E., Vionnet, V., Boone, A., Decharme, B., Peings, Y., Valette, R., Karbou, F., and Morin, S.: Simulation of northern Eurasian local snow depth, mass, and density using a detailed snowpack model and meteorological reanalyses, Journal of Hydrometeorology, 14, 203–219, https://doi.org/10.1175/JHM-D-12-012.1, 2013.

Brunet, Y.: Turbulent Flow in Plant Canopies: Historical Perspective and Overview, vol. 177, Springer Netherlands, https://doi.org/10.1007/s10546-020-00560-7, 2020.

Caillaud, C., Somot, S., Alias, A., Bernard-Bouissières, I., Fumière, Q., Laurantin, O., Seity, Y., and Ducrocq, V.: Modelling Mediterranean heavy precipitation events at climate scale: an object-oriented evaluation of the CNRM-AROME convection-permitting regional climate model, vol. 56, Springer Berlin Heidelberg, https://doi.org/10.1007/s00382-020-05558-y, 2021.

Calvet, J. C., Noilhan, J., Roujean, J. L., Bessemoulin, P., Cabelguenne, M., Olioso, A., and Wigneron, J. P.: An interactive vegetation SVAT model tested against data from six contrasting sites, Agricultural and Forest Meteorology, 92, 73–95, https://doi.org/10.1016/S0168-1923(98)00091-4, 1998.

Carrer, D., Roujean, J. L., Lafont, S., Calvet, J. C., Boone, A., Decharme, B., Delire, C., and Gastellu-Etchegorry, J. P.: A canopy radiative transfer scheme with explicit FAPAR for the interactive vegetation model ISBA-A-gs: Impact on carbon fluxes, Journal of Geophysical Research: Biogeosciences, 118, 888–903, https://doi.org/10.1002/jgrg.20070, 2013.

Chadburn, S., Burke, E., Essery, R., Boike, J., Langer, M., Heikenfeld, M., Cox, P., and Friedlingstein, P.: An improved representation of physical permafrost dynamics in the JULES land-surface model, Geoscientific Model Development, 8, 1493–1508, https://doi.org/10.5194/gmd-8-1493-2015, 2015.

Champeaux, J. L., Masson, V., and Chauvin, F.: ECOCLIMAP: A global database of land surface parameters at 1 km resolution, Meteorological Applications, 12, 29–32, https://doi.org/10.1017/S1350482705001519, 2005.

Clark, M. P., Hendrikx, J., Slater, A. G., Kavetski, D., Anderson, B., Cullen, N. J., Kerr, T., Örn Hreinsson, E., and Woods, R. A.: Representing spatial variability of snow water equivalent in hydrologic and land-surface models: A review, Water Resources Research, 47, https://doi.org/10.1029/2011WR010745, 2011.

Clark, M. P., Nijssen, B., Lundquist, J. D., Kavetski, D., Rupp, D. E., Woods, R. A., Freer, J. E., Gutmann, E. D., Wood, A. W., Brekke, L. D., Arnold, J. R., Gochis, D. J., and Rasmussen, R. M.: A unified approach for process-based hydrologic modeling: 1. Modeling concept, Water Resources Research, 51, 2498–2514, https://doi.org/10.1002/2015WR017200.A, 2015.

Cohen, J. and Rind, D.: The Effect of Snow Cover on the Climate, Journal of Climate, 4, 689–706, https://doi.org/10.1175/1520-0442(1991)004<0689:TEOSCO>2.0.CO;2, 1991.

Conway, J. P., Pomeroy, J. W., Helgason, W. D., and Kinar, N. J.: Challenges in modeling turbulent heat fluxes to snowpacks in forest clearings, Journal of Hydrometeorology, 19, 1599–1616, https://doi.org/10.1175/JHM-D-18-0050.1, 2018.

Couet, J., Marjakangas, E. L., Santangeli, A., Kålås, J. A., Lindström, , and Lehikoinen, A.: Short-lived species move uphill faster under climate change, Oecologia, https://doi.org/10.1007/s00442-021-05094-4, 2022.

Courtier, P., Freydier, C., Geleyn, J.-F., Rabier, F., and Rochas, M.: The Arpege project at Météo-France, 1991.

Dankers, R., Burke, E. J., and Price, J.: Simulation of permafrost and seasonal thaw depth in the JULES land surface scheme, Cryosphere, 5, 773–790, https://doi.org/10.5194/tc-5-773-2011, 2011.

Decharme, B., Boone, A., Delire, C., and Noilhan, J.: Local evaluation of the Interaction between Soil Biosphere Atmosphere soil multilayer diffusion scheme using four pedotransfer functions, Journal of Geophysical Research Atmospheres, 116, 1–29, https://doi.org/10.1029/2011JD016002, 2011.

Decharme, B., Brun, E., Boone, A., Delire, C., Le Moigne, P., and Morin, S.: Impacts of snow and organic soils parameterization on northern Eurasian soil temperature profiles simulated by the ISBA land surface model, Cryosphere, 10, 853–877, https://doi.org/10.5194/tc-10-853-2016, 2016.

Decharme, B., Delire, C., Minvielle, M., Colin, J., Vergnes, J. P., Alias, A., Saint-Martin, D., Séférian, R., Sénési, S., and Voldoire, A.: Recent Changes in the ISBA-CTRIP Land Surface System for Use in the CNRM-CM6 Climate Model and in Global Off-Line Hydrological Applications, Journal of Advances in Modeling Earth Systems, 11, 1207–1252, https://doi.org/10.1029/2018MS001545, 2019.

Derbyshire, S. H.: Boundary-layer decoupling over cold surfaces as a physical boundary-instability, Boundary-Layer Meteorology, 90, 297–325, https://doi.org/10.1023/A:1001710014316, 1999.

Deschamps-Berger, C., Cluzet, B., Dumont, M., Lafaysse, M., Berthier, E., Fanise, P., and Gascoin, S.: Improving the Spatial Distribution of Snow Cover Simulations by Assimilation of Satellite Stereoscopic Imagery, Water Resources Research, 58, https://doi.org/10.1029/2021WR030271, 2022.

Domine, F., Belke-Brea, M., Sarrazin, D., Arnaud, L., Barrere, M., and Poirier, M.: Soil moisture, wind speed and depth hoar formation in the Arctic snowpack, Journal of Glaciology, 64, 990–1002, https://doi.org/10.1017/jog.2018.89, 2018.

Douville, H., Royer, J. F., and Mahfouf, J. F.: A new snow parameterization for the Météo-France climate model, Climate Dynamics, 12, 21–35, https://doi.org/10.1007/BF00208760, 1995.

Esri: ESRI Satellite (ArcGIS/World_Imagery), https://www.arcgis.com/home/item.html?id=10df2279f9684e4a9f6a7f08febac2a9, 2023.

Essery, R., Rutter, N., Pomeroy, J., Baxter, R., Stahli, M., Gustafsson, D., Barr, A., Bartlett, P., and Elder, K.: SnowMIP2: An evalution of forest snow process simulation, Bulletin of the American Meteorological Society, 90, 1130–1135, https://doi.org/10.1175/2009BAMS2629.1, 2009.

Eugster, W., Rouse, W. R., Pielke, R. A., Mcfadden, J. P., Baldocchi, D. D., Kittel, T. G., Chapin, F. S., Liston, G. E., Vidale, P. L., Vaganov, E., and Chambers, S.: Land-atmosphere energy exchange in Arctic tundra and boreal forest: Available data and feedbacks to climate, Global Change Biology, 6, 84–115, https://doi.org/10.1046/j.1365-2486.2000.06015.x, 2000.

Faroux, S., Kaptué Tchuenté, A. T., Roujean, J.-L., Masson, V., Martin, E., and Le Moigne, P.: ECOCLIMAP-II/Europe: a twofold database of ecosystems and surface parameters at 1 km resolution based on satellite information for use in land surface, meteorological and climate models, Geoscientific Model Development, 6, 563–582, https://doi.org/10.5194/gmd-6-563-2013, 2013.

FMI: Finnish Meteorological Institute past weather observations, available at: https://en.ilmatieteenlaitos.fi/download-observations, 2021.

Foken, T., Göockede, M., Mauder, M., Mahrt, L., Amiro, B., and Munger, W.: Post-Field Data Quality Control, in: Handbook of Micrometeorology: A Guide for Surface Flux Measurement and Analysis, edited by Lee, X., Massman, W., and Law, B., pp. 181–208, Springer Netherlands, Dordrecht, https://doi.org/10.1007/1-4020-2265-4_9, 2005.

Gouttevin, I., Lehning, M., Jonas, T., Gustafsson, D., and Mölder, M.: A two-layer canopy model with thermal inertia for an improved snowpack energy balance below needleleaf forest (model SNOWPACK, version 3.2.1, revision 741), Geoscientific Model Development, 8, 2379–2398, https://doi.org/10.5194/gmd-8-2379-2015, 2015.

Gouttevin, I., Vionnet, V., Seity, Y., Boone, A., Lafaysse, M., Deliot, Y., and Merzisen, H.: To the Origin of a Wintertime Screen-Level Temperature Bias at High Altitude in a Kilometric NWP Model, Journal of Hydrometeorology, 24, 53–71, https://doi.org/10.1175/JHM-D-21-0200.1, 2023.

Hamdi, R., Degrauwe, D., Duerinckx, A., Cedilnik, J., Costa, V., Dalkilic, T., Essaouini, K., Jerczynki, M., Kocaman, F., Kullmann, L., Mahfouf, J. F., Meier, F., Sassi, M., Schneider, S., Váňa, F., and Termonia, P.: Evaluating the performance of SURFEXv5 as a new land surface scheme for the ALADINcy36 and ALARO-0 models, Geoscientific Model Development, 7, 23–39, https://doi.org/10.5194/gmd-7-23-2014, 2014.

Hari, P., Nikinmaa, E., Pohja, T., Siivola, E., Bäck, J., Vesala, T., and Kulmala, M.: Station for measuring ecosystem-atmosphere relations: SMEAR, Physical and Physiological Forest Ecology, 9789400756, 471–487, https://doi.org/10.1007/978-94-007-5603-8_9, 2013.

Hersbach, H., Bell, B., Berrisford, P., Hirahara, S., Horányi, A., Muñoz-Sabater, J., Nicolas, J., Peubey, C., Radu, R., Schepers, D., Simmons, A., Soci, C., Abdalla, S., Abellan, X., Balsamo, G., Bechtold, P., Biavati, G., Bidlot, J., Bonavita, M., De Chiara, G., Dahlgren, P., Dee, D., Diamantakis, M., Dragani, R., Flemming, J., Forbes, R., Fuentes, M., Geer, A., Haimberger, L., Healy, S., Hogan, R. J., Hólm, E., Janisková, M., Keeley, S., Laloyaux, P., Lopez, P., Lupu, C., Radnoti, G., de Rosnay, P., Rozum, I., Vamborg, F., Villaume, S., and Thépaut, J. N.: The ERA5 global reanalysis, Quarterly Journal of the Royal Meteorological Society, 146, 1999–2049, https://doi.org/10.1002/qj.3803, 2020.

Jordan, R. E., Andreas, E. L., and Makshtas, A. P.: Heat budget of snow-covered sea ice at North Pole 4, Journal of Geophysical Research: Oceans, 104, 7785–7806, https://doi.org/10.1029/1999jc900011, 1999.

Koivusalo, H. and Heikinheimo, M.: Surface energy exchange over a boreal snowpack: Comparison of two snow energy balance models, Hydrological Processes, 13, 2395–2408, https://doi.org/10.1002/(SICI)1099-1085(199910)13:14/15<2395::AID-HYP864>3.0.CO;2-G, 1999.

Kolari, P., Aalto, J., Levula, J., Kulmala, L., Ilvesniemi, H., and Pumpanen, J.: Hyytiälä SMEAR II site characteristics, https://doi.org/10.5281/zenodo.5909681, 2022.

Kreyling, J., Haei, M., and Laudon, H.: Absence of snow cover reduces understory plant cover and alters plant community composition in boreal forests, Oecologia, 168, 577–587, https://doi.org/10.1007/s00442-011-2092-z, 2012.

Krinner, G., Derksen, C., Essery, R., Flanner, M., Hagemann, S., Clark, M., Hall, A., Rott, H., Brutel-Vuilmet, C., Kim, H., Ménard, C. B., Mudryk, L., Thackeray, C., Wang, L., Arduini, G., Balsamo, G., Bartlett, P., Boike, J., Boone, A., Chéruy, F., Colin, J., Cuntz, M., Dai, Y., Decharme, B., Derry, J., Ducharne, A., Dutra, E., Fang, X., Fierz, C., Ghattas, J., Gusev, Y., Haverd, V., Kontu, A., Lafaysse, M., Law, R., Lawrence, D., Li, W., Marke, T., Marks, D., Ménégoz, M., Nasonova, O., Nitta, T., Niwano, M., Pomeroy, J., Raleigh, M. S., Schaedler,

G., Semenov, V., Smirnova, T. G., Stacke, T., Strasser, U., Svenson, S., Turkov, D., Wang, T., Wever, N., Yuan, H., Zhou, W., and Zhu, D.: ESM-SnowMIP: Assessing snow models and quantifying snow-related climate feedbacks, Geoscientific Model Development, 11, 5027–5049, https://doi.org/10.5194/gmd-11-5027-2018, 2018.

Lackner, G., Dominé, F., Nadeau, D., Parent, A.-C., Anctil, F., Lafaysse, M., and Dumont, M.: On the energy budget of a low-Arctic snowpack, The Cryosphere Discussions, pp. 1–27, https://doi.org/10.5194/tc-2021-255, 2021.

Lafaysse, M., Hingray, B., Etchevers, P., Martin, E., and Obled, C.: Influence of spatial discretization, underground water storage and glacier melt on a physically-based hydrological model of the Upper Durance River basin, Journal of Hydrology, 403, 116–129, https://doi.org/10.1016/j.jhydrol.2011.03.046, 2011.

Lafaysse, M., Cluzet, B., Dumont, M., Lejeune, Y., Vionnet, V., and Morin, S.: A multiphysical ensemble system of numerical snow modelling, Cryosphere, 11, 1173–1198, https://doi.org/10.5194/tc-11-1173-2017, 2017.

Langer, M., Westermann, S., Muster, S., Piel, K., and Boike, J.: The surface energy balance of a polygonal tundra site in northern Siberia - Part 2: Winter, Cryosphere, 5, 509–524, https://doi.org/10.5194/tc-5-509-2011, 2011.

Lapo, K., Nijssen, B., and Lundquist, J. D.: Evaluation of Turbulence Stability Schemes of Land Models for Stable Conditions, Journal of Geophysical Research: Atmospheres, 124, 3072–3089, https://doi.org/10.1029/2018JD028970, 2019.

Launiainen, S.: Seasonal and inter-annual variability of energy exchange above a boreal Scots pine forest, Biogeosciences, 7, 3921–3940, https://doi.org/10.5194/bg-7-3921-2010, 2010.

Launiainen, S., Katul, G. G., Lauren, A., and Kolari, P.: Coupling boreal forest CO2, H2O and energy flows by a vertically structured forest canopy - Soil model with separate bryophyte layer, Ecological Modelling, 312, 385–405, https://doi.org/10.1016/j.ecolmodel.2015.06.007, 2015.

Launiainen, S., Katul, G. G., Leppä, K., Kolari, P., Aslan, T., Grönholm, T., Korhonen, L., Mammarella, I., and Vesala, T.: Does growing atmospheric CO2 explain increasing carbon sink in a boreal coniferous forest?, Global Change Biology, 28, 2910–2929, https://doi.org/10.1111/gcb.16117, 2022.

Lawrence, D. M. and Slater, A. G.: Incorporating organic soil into a global climate model, Climate Dynamics, 30, 145–160, https://doi.org/10.1007/s00382-007-0278-1, 2008.

Lawrence, D. M., Fisher, R. A., Koven, C. D., Oleson, K. W., Swenson, S. C., Bonan, G., Collier, N., Ghimire, B., van Kampenhout, L., Kennedy, D., Kluzek, E., Lawrence, P. J., Li, F., Li, H., Lombardozzi, D., Riley, W. J., Sacks, W. J., Shi, M., Vertenstein, M., Wieder, W. R., Xu, C., Ali, A. A., Badger, A. M., Bisht, G., van den Broeke, M., Brunke, M. A., Burns, S. P., Buzan, J., Clark, M., Craig, A., Dahlin, K., Drewniak, B., Fisher, J. B., Flanner, M., Fox, A. M., Gentine, P., Hoffman, F., Keppel-Aleks, G., Knox, R., Kumar, S., Lenaerts, J., Leung, L. R., Lipscomb, W. H., Lu, Y., Pandey, A., Pelletier, J. D., Perket, J., Randerson, J. T., Ricciuto, D. M., Sanderson, B. M., Slater, A., Subin, Z. M., Tang, J., Thomas, R. Q., Val Martin, M., and Zeng, X.: The Community Land Model Version 5: Description of New Features, Benchmarking, and Impact of Forcing Uncertainty, Journal of Advances in Modeling Earth Systems, 11, 4245–4287, https://doi.org/10.1029/2018MS001583, 2019.

Le Moigne, P., Besson, F., Martin, E., Boé, J., Boone, A., Decharme, B., Etchevers, P., Faroux, S., Habets, F., Lafaysse, M., Leroux, D., and Rousset-Regimbeau, F.: The latest improvements with SURFEX v8.0 of the Safran-Isba-Modcou hydrometeorological model for France, Geoscientific Model Development, 13, 3925–3946, https://doi.org/10.5194/gmd-13-3925-2020, 2020.

Lindroos, A. J., Mäkipää, R., and Merilä, P.: Soil carbon stock changes over 21 years in intensively monitored boreal forest stands in Finland, Ecological Indicators, 144, https://doi.org/10.1016/j.ecolind.2022.109551, 2022.

Liston, G. E. and Sturm, M.: Winter precipitation patterns in arctic Alaska determined from a blowing-snow model and snow-depth observations, Journal of Hydrometeorology, 3, 646–659, https://doi.org/10.1175/1525-7541(2002)003<0646:WPPIAA>2.0.CO;2, 2002.

Lohila, A., Penttilä, T., Jortikka, S., Aalto, T., Anttila, P., Asmi, E., Aurela, M., Hatakka, J., Hellén, H., Henttonen, H., Hänninen, P., Kilkki, J., Kyllönen, K., Laurila, T., Lepistö, A., Lihavainen, H., Makkonen, U., Paatero, J., Rask, M., Sutinen, R., Tuovinen, J. P., Vuorenmaa, J., and Viisanen, Y.: Preface to the special issue on integrated research of atmosphere, ecosystems and environment at Pallas, Boreal Environment Research, 20, 431–454, 2015.

Loranty, M. M., Berner, L. T., Goetz, S. J., Jin, Y., and Randerson, J. T.: Vegetation controls on northern high latitude snow-albedo feedback: Observations and CMIP5 model simulations, Global Change Biology, 20, 594–606, https://doi.org/10.1111/gcb.12391, 2014.

Louis, J. F.: A parametric model of vertical eddy fluxes in the atmosphere, Boundary-Layer Meteorology, 17, 187–202, https://doi.org/10.1007/BF00117978, 1979.

Lundquist, J. D., Dickerson-Lange, S. E., Lutz, J. A., and Cristea, N. C.: Lower forest density enhances snow retention in regions with warmer winters: A global framework developed from plot-scale observations and modeling, Water Resources Research, 49, 6356–6370, https://doi.org/10.1002/wrcr.20504, 2013.

Lundquist, J. D., Dickerson-Lange, S., Gutmann, E., Jonas, T., Lumbrazo, C., and Reynolds, D.: Snow interception modelling: Isolated observations have led to many land surface models lacking appropriate temperature sensitivities, Hydrological Processes, 35, 1–20, https://doi.org/10.1002/hyp.14274, 2021.

Mahfouf, A. J., Manzi, A. O., Noilhan, J., Giordani, H., and Déqué, M.: The Land Surface Scheme ISBA within the Météo-France Climate Model ARPEGE . Part I : Implementation and Preliminary Results Published by : American Meteorological Society Stable URL : http://www.jstor.com/stable/26200036 REFERENCES Linked references are a, 8, 2039–2057, 1995.

Malle, J., Rutter, N., Webster, C., Mazzotti, G., Wake, L., and Jonas, T.: Effect of Forest Canopy Structure on Wintertime Land Surface Albedo: Evaluating CLM5 Simulations With In-Situ Measurements, Journal of Geophysical Research: Atmospheres, 126, 1–15, https://doi.org/10.1029/2020JD034118, 2021.

Mammarella, I., Peltola, O., Nordbo, A., and Järvi, L.: Quantifying the uncertainty of eddy covariance fluxes due to the use of different software packages and combinations of processing steps in two contrasting ecosystems, Atmospheric Measurement Techniques, 9, 4915–4933, https://doi.org/10.5194/amt-9-4915-2016, 2016.

Mammarella, I., Rannik, , Launiainen, S., Alekseychik, P., Peltola, O., Keronen, P., Kolari, P., Laakso, H., Matilainen, T., Salminen, T., and others: SMEAR II Hyytiälä forest eddy covariance, \url{https://doi.org/10.23729/40f64739-11d1-4e5f-8dc2-da931512c91c}, 2019.

Martin, E. and Lejeune, Y.: Turbulent fluxes above the snow surface, Annals of Glaciology, 26, 179–183, https://doi.org/10.3189/1998aog26-1-179-183, 1998.

Marttila, H., Lohila, A., Ala-Aho, P., Noor, K., Welker, J. M., Croghan, D., Mustonen, K., Meriö, L., Autio, A., Muhic, F., Bailey, H., Aurela, M., Vuorenmaa, J., Penttilä, T., Hyöky, V., Klein, E., Kuzmin, A., Korpelainen, P., Kumpula, T., Rauhala, A., and Kløve, B.: Subarctic catchment water storage and carbon cycling – Leading the way for future studies using integrated datasets at Pallas, Finland, Hydrological Processes, 35, 1–19, https://doi.org/10.1002/hyp.14350, 2021.

Masson, V., Le Moigne, P., Martin, E., Faroux, S., Alias, A., Alkama, R., Belamari, S., Barbu, A., Boone, A., Bouyssel, F., Brousseau, P., Brun, E., Calvet, J. C., Carrer, D., Decharme, B., Delire, C., Donier, S., Essaouini, K., Gibelin, A. L., Giordani, H., Habets, F., Jidane, M., Kerdraon, G., Kourzeneva, E., Lafaysse, M., Lafont, S., Lebeaupin Brossier, C., Lemonsu, A., Mahfouf, J. F., Marguinaud, P., Mokhtari, M., Morin, S., Pigeon, G., Salgado, R., Seity, Y., Taillefer, F., Tanguy, G., Tulet, P., Vincendon, B., Vionnet, V., and Voldoire, A.: The

SURFEXv7.2 land and ocean surface platform for coupled or offline simulation of earth surface variables and fluxes, Geoscientific Model Development, 6, 929–960, https://doi.org/10.5194/gmd-6-929-2013, 2013.

Mauder, M., Foken, T., and Cuxart, J.: Surface-Energy-Balance Closure over Land: A Review, vol. 177, Springer Netherlands, https://doi.org/10.1007/s10546-020-00529-6, 2020.

Mazzotti, G., Essery, R., Moeser, C. D., and Jonas, T.: Resolving Small-Scale Forest Snow Patterns Using an Energy Balance Snow Model With a One-Layer Canopy, Water Resources Research, 56, https://doi.org/10.1029/2019WR026129, 2020a.

Mazzotti, G., Essery, R., Webster, C., Malle, J., and Jonas, T.: Process-Level Evaluation of a Hyper-Resolution Forest Snow Model Using Distributed Multisensor Observations, Water Resources Research, 56, 1–25, https://doi.org/10.1029/2020WR027572, 2020b.

Mazzotti, G., Webster, C., Essery, R., and Jonas, T.: Increasing the Physical Representation of Forest-Snow Processes in Coarse-Resolution Models: Lessons Learned From Upscaling Hyper-Resolution Simulations, Water Resources Research, 57, 1–21, https://doi.org/10.1029/2020WR029064, 2021.

McGowan, L. E., Paw U, K. T., and Dahlke, H. E.: What Does a Multilayer Canopy Model Tell Us About Our Current Understanding of Snow-Canopy Unloading?, in: AGU Fall Meeting Abstracts, vol. 2017, pp. C43B–06, 2017.

Ménard, C. B., Essery, R., Barr, A., Bartlett, P., Derry, J., Dumont, M., Fierz, C., Kim, H., Kontu, A., Lejeune, Y., Marks, D., Niwano, M., Raleigh, M., Wang, L., and Wever, N.: Meteorological and evaluation datasets for snow modelling at 10 reference sites: Description of in situ and bias-corrected reanalysis data, Earth System Science Data, 11, 865–880, https://doi.org/10.5194/essd-11-865-2019, 2019.

Menard, C. B., Essery, R., Krinner, G., Arduini, G., Bartlett, P., Boone, A., Brutel-Vuilmet, C., Burke, E., Cuntz, M., Dai, Y., Decharme, B., Dutra, E., Fang, X., Fierz, C., Gusev, Y., Hagemann, S., Haverd, V., Kim, H., Lafaysse, M., Marke, T., Nasonova, O., Nitta, T., Niwano, M., Pomeroy, J., Schädler, G., Semenov, V. A., Smirnova, T., Strasser, U., Swenson, S., Turkov, D., Wever, N., and Yuan, H.: Scientific and human errors in a snow model intercomparison, Bulletin of the American Meteorological Society, 102, E61–E79, https://doi.org/10.1175/BAMS-D-19-0329.1, 2021.

Menberu, M. W., Marttila, H., Ronkanen, A. K., Haghighi, A. T., and Kløve, B.: Hydraulic and Physical Properties of Managed and Intact Peatlands: Application of the Van Genuchten-Mualem Models to Peat Soils, Water Resources Research, 57, 1–22, https://doi.org/10.1029/2020WR028624, 2021.

Meriö, L.-J., Rauhala, A., Ala-aho, P., Kuzmin, A., Korpelainen, P., Kumpula, T., Kløve, B., and Marttila, H.: Measuring the spatiotemporal variability of snow depth in subarctic environments using unmanned aircraft systems (UAS) – Part 2: Snow processes and snow-canopy interactions, The Cryosphere Discussions, 2023, 1–28, https://doi.org/10.5194/tc-2022-242, 2023.

Molotch, N. P., Blanken, P. D., Williams, M. W., Turnipseed, A. A., Monson, R. K., and Margulis, S. A.: Estimating sublimation of intercepted and sub-canopy snow using eddy covariance systems, Hydrological Processes: An International Journal, 21, 1567–1575, 2009.

Morin, S., Horton, S., Techel, F., Bavay, M., Coléou, C., Fierz, C., Gobiet, A., Hagenmuller, P., Lafaysse, M., Ližar, M., Mitterer, C., Monti, F., Müller, K., Olefs, M., Snook, J. S., van Herwijnen, A., and Vionnet, V.: Application of physical snowpack models in support of operational avalanche hazard forecasting: A status report on current implementations and prospects for the future, Cold Regions Science and Technology, 170, 102 910, https://doi.org/10.1016/j.coldregions.2019.102910, 2020.

Morris, P. J., Davies, M. L., Baird, A. J., Balliston, N., Bourgault, M., Clymo, R. S., Fewster, R. E., Furukawa, A. K., Holden, J., Kessel, E., Ketcheson, S. J., Kløve, B., Larocque, M., Marttila, H., Menberu, M. W., Moore, P. A., Price, J. S., Ronkanen, A., Rosa, E., Strack, M., Surridge, B. W. J., Waddington, J. M., Whittington, P., and Wilkinson, S. L.: Saturated Hydraulic Conductivity in Northern Peats Inferred From Other Measurements, Water Resources Research, 58, https://doi.org/10.1029/2022wr033181, 2022.

Muhic, F., Ala-Aho, P., Noor, K., Welker, J. M., Klöve, B., and Marttila, H.: Flushing or mixing? Stable water isotopes reveal differences in arctic forest and peatland soil water seasonality, Hydrological Processes, 37, 1–22, https://doi.org/10.1002/hyp.14811, 2023.

Mustamo, P., Ronkanen, A. K., Berglund, , Berglund, K., and Kløve, B.: Thermal conductivity of unfrozen and partially frozen managed peat soils, Soil and Tillage Research, 191, 245–255, https://doi.org/10.1016/j.still.2019.02.017, 2019.

Nabat, P., Somot, S., Cassou, C., Mallet, M., Michou, M., Bouniol, D., Decharme, B., Drugé, T., Roehrig, R., and Saint-Martin, D.: Modulation of radiative aerosols effects by atmospheric circulation over the Euro-Mediterranean region, Atmospheric Chemistry and Physics, 20, 8315–8349, https://doi.org/10.5194/acp-20-8315-2020, 2020.

Napoly, A., Boone, A., Samuelsson, P., Gollvik, S., Martin, E., Seferian, R., Carrer, D., Decharme, B., and Jarlan, L.: The interactions between soil-biosphere-atmosphere (ISBA) land surface model multi-energy balance (MEB) option in SURFEXv8 - Part 2: Introduction of a litter formulation and model evaluation for local-scale forest sites, Geoscientific Model Development, 10, 1621–1644, https://doi.org/10.5194/gmd-10-1621-2017, 2017.

Napoly, A., Boone, A., and Welfringer, T.: ISBA-MEB (SURFEX v8.1): model snow evaluation for local-scale forest sites, Geoscientific Model Development, 13, 6523–6545, 2020.

Nicolsky, D. J., Romanovsky, V. E., Alexeev, V. A., and Lawrence, D. M.: Improved modeling of permafrost dynamics in a GCM land-surface scheme, Geophysical Research Letters, 34, 2–6, https://doi.org/10.1029/2007GL029525, 2007.

Niu, G. Y., Yang, Z. L., Mitchell, K. E., Chen, F., Ek, M. B., Barlage, M., Kumar, A., Manning, K., Niyogi, D., Rosero, E., Tewari, M., and Xia, Y.: The community Noah land surface model with multiparameterization options (Noah-MP): 1. Model description and evaluation with local-scale measurements, Journal of Geophysical Research Atmospheres, 116, 1–19, https://doi.org/10.1029/2010JD015139, 2011.

NLSF: National Land Survey of Finland Topographic Database, available at: http://www.maanmittauslaitos.fi/en/e-services/open-data-file-download-service, 2020.

Noilhan, J. and Mahfouf, J. F.: The ISBA land surface parameterisation scheme, Global and Planetary Change, 13, 145–159, https://doi.org/10.1016/0921-8181(95)00043-7, 1996.

Noilhan, J. and Planton, S.: A simple parameterization of land surface processes for meteorological models, Monthly Weather Review, 117, 536–549, https://doi.org/10.1175/1520-0493(1989)117<0536:ASPOLS>2.0.CO;2, 1989.

Noor, K., Marttila, H., Klöve, B., Welker, J. M., and Ala-aho, P.: The Spatiotemporal Variability of Snowpack and Snowmelt Water O and H Isotopes in a Subarctic Catchment Water Resources Research, Water Resources Research, 59, 1–19, https://doi.org/10.1029/2022WR033101, 2022.

Nousu, J. P., Lafaysse, M., Vernay, M., Bellier, J., Evin, G., and Joly, B.: Statistical post-processing of ensemble forecasts of the height of new snow, Nonlinear Processes in Geophysics, 26, 339–357, https://doi.org/10.5194/npg-26-339-2019, 2019.

Olson, D. M., Dinerstein, E., Wikramanayake, E. D., Burgess, N. D., Powell, G. V., Underwood, E. C., D'Amico, J. A., Itoua, I., Strand, H. E., Morrison, J. C., Loucks, C. J., Allnutt, T. F., Ricketts, T. H., Kura, Y., Lamoreux, J. F., Wettengel, W. W., Hedao, P., and Kassem, K. R.: Terrestrial ecoregions of the world: A new map of life on Earth, BioScience, 51, 933–938, https://doi.org/10.1641/0006-3568(2001)051[0933:TEOTWA]2.0.CO;2, 2001.

Park, H., Launiainen, S., Konstantinov, P. Y., Iijima, Y., and Fedorov, A. N.: Modeling the Effect of Moss Cover on Soil Temperature and Carbon Fluxes at a Tundra Site in Northeastern Siberia, Journal of Geophysical Research: Biogeosciences, 123, 3028–3044, https://doi.org/10.1029/2018JG004491, 2018.

Pedersen, S. H., Bentzen, T. W., Reinking, A. K., Liston, G. E., Elder, K., Lenart, E. A., Prichard, A. K., and Welker, J. M.: Quantifying effects of snow depth on caribou winter range selection and movement in Arctic Alaska, Movement Ecology, 9, 1–24, https://doi.org/10.1186/s40462-021-00276-4, 2021.

Peters-Lidard, C. D., Blackburn, E., Liang, X., and Wood, E. F.: The effect of soil thermal conductivity parameterization on surface energy fluxes and temperatures, Journal of the Atmospheric Sciences, 55, 1209–1224, https://doi.org/10.1175/1520-0469(1998)055<1209:TEOSTC>2.0.CO;2, 1998.

Pomeroy, J. W. and Dion, K.: Winter radiation extinction and reflection in a boreal pine canopy: Measurements and modelling, Hydrological Processes, 10, 1591–1608, https://doi.org/10.1002/(sici)1099-1085(199612)10:12<1591::aid-hyp503>3.0.co;2-8, 1996.

Pomeroy, J. W. and Essery, R. L.: Turbulent fluxes during blowing snow: Field tests of model sublimation predictions, Hydrological Processes, 13, 2963–2975, https://doi.org/10.1002/(SICI)1099-1085(19991230)13:18<2963::AID-HYP11>3.0.CO;2-9, 1999.

Raleigh, M. S., Lundquist, J. D., and Clark, M. P.: Exploring the impact of forcing error characteristics on physically based snow simulations within a global sensitivity analysis framework, Hydrology and Earth System Sciences, 19, 3153–3179, https://doi.org/10.5194/hess-19-3153-2015, 2015.

Rantanen, M., Karpechko, A. Y., Lipponen, A., Nordling, K., Hyvärinen, O., Ruosteenoja, K., Vihma, T., and Laaksonen, A.: The Arctic has warmed nearly four times faster than the globe since 1979, Communications Earth and Environment, 3, 1–10, https://doi.org/10.1038/s43247-022-00498-3, 2022.

Rasmus, S., Lundell, R., and Saarinen, T.: Interactions between snow, canopy, and vegetation in a boreal coniferous forest, Plant Ecology and Diversity, 4, 55–65, https://doi.org/10.1080/17550874.2011.558126, 2011.

Reba, M. L., Link, T. E., Marks, D., and Pomeroy, J.: An assessment of corrections for eddy covariance measured turbulent fluxes over snow in mountain environments, Water Resources Research, 46, https://doi.org/10.1029/2008WR007045, 2009.

Revuelto, J., Lecourt, G., Lafaysse, M., Zin, I., Charrois, L., Vionnet, V., Dumont, M., Rabatel, A., Six, D., Condom, T., Morin, S., Viani, A., and Sirguey, P.: Multi-criteria evaluation of snowpack simulations in complex alpine terrain using satellite and in situ observations, Remote Sensing, 10, 1–32, https://doi.org/10.3390/rs10081171, 2018.

Ricchiazzi, P., Yang, S., Gautier, C., and Sowle, D.: SBDART: A Research and Teaching Software Tool for Plane-Parallel Radiative Transfer in the Earth's Atmosphere, Bulletin of the American Meteorological Society, 79, 2101–2114, https://doi.org/10.1175/1520-0477(1998)079<2101:SARATS>2.0.CO;2, 1998.

Richter, B., Schweizer, J., Rotach, M. W., and Van Herwijnen, A.: Modeling spatially distributed snow instability at a regional scale using Alpine3D, Journal of Glaciology, 67, 1147–1162, https://doi.org/10.1017/jog.2021.61, 2021.

Rinne, J., Tuittila, E. S., Peltola, O., Li, X., Raivonen, M., Alekseychik, P., Haapanala, S., Pihlatie, M., Aurela, M., Mammarella, I., and Vesala, T.: Temporal Variation of Ecosystem Scale Methane Emission From a Boreal Fen in Relation to Temperature, Water Table Position, and Carbon Dioxide Fluxes, Global Biogeochemical Cycles, 32, 1087–1106, https://doi.org/10.1029/2017GB005747, 2018.

Rissanen, T., Niittynen, P., Soininen, J., and Luoto, M.: Snow information is required in subcontinental scale predictions of mountain plant distributions, Global Ecology and Biogeography, 30, 1502–1513, https://doi.org/10.1111/geb.13315, 2021.

Rutter, N., Essery, R., Pomeroy, J., Altimir, N., Andreadis, K., Baker, I., Barr, A., Bartlett, P., Boone, A., Deng, H., Douville, H., Dutra, E., Elder, K., Ellis, C., Feng, X., Gelfan, A., Goodbody, A., Gusev, Y., Gustafsson, D., Hellström, R., Hirabayashi, Y., Hirota, T., Jonas, T., Koren, V., Kuragina, A., Lettenmaier, D., Li, W. P., Luce, C., Martin, E., Nasonova, O., Pumpanen, J., Pyles, R. D., Samuelsson, P., Sandells, M., Schädler, G., Shmakin, A., Smirnova, T. G., Stähli, M., Stöckli, R., Strasser, U., Su, H., Suzuki, K., Takata, K., Tanaka,

K., Thompson, E., Vesala, T., Viterbo, P., Wiltshire, A., Xia, K., Xue, Y., and Yamazaki, T.: Evaluation of forest snow processes models (SnowMIP2), Journal of Geophysical Research Atmospheres, 114, https://doi.org/10.1029/2008JD011063, 2009.

Salas-Mélia, D., Chauvin, F., Déqué, M., Douville, H., Gueremy, J., Marquet, P., Planton, S., Royer, J., and Tyteca, S.: Description and validation of the CNRM-CM3 global coupled model., CNRM working note 103, p. 36, http://www.cnrm.meteo.fr/scenario2004/paper_cm3.pdf, 2005.

Screen, J. A. and Simmonds, I.: The central role of diminishing sea ice in recent Arctic temperature amplification, Nature, 464, 1334–1337, https://doi.org/10.1038/nature09051, 2010.

Serreze, M. C., Barrett, A. P., Stroeve, J. C., Kindig, D. N., and Holland, M. M.: The emergence of surface-based Arctic amplification, Cryosphere, 3, 11–19, https://doi.org/10.5194/tc-3-11-2009, 2009.

Slater, A. G., Schlosser, C. A., Desborough, C. E., Pitman, A. J., Henderson-Sellers, A., Robock, A., Vinnikov, K. Y., Mitchell, K., Boone, A., Braden, H., Chen, F., Cox, P. M., De Rosnay, P., Dickinson, R. E., Dai, Y. J., Duan, Q., Entin, J., Etchevers, P., Gedney, N., Gusev, Y. M., Habets, F., Kim, J., Koren, V., Kowalczyk, E. A., Nasonova, O. N., Noilhan, J., Schaake, S., Shmakin, A. B., Smirnova, T. G., Verseghy, D., Wetzel, P., Xue, Y., Yang, Z. L., and Zeng, Q.: The representation of snow in land surface schemes: Results from PILPS 2(d), Journal of Hydrometeorology, 2, 7–25, https://doi.org/10.1175/1525-7541(2001)002<0007:TROSIL>2.0.CO;2, 2001.

Stiegler, C., Lund, M., Røjle Christensen, T., Mastepanov, M., and Lindroth, A.: Two years with extreme and little snowfall: Effects on energy partitioning and surface energy exchange in a high-Arctic tundra ecosystem, Cryosphere, 10, 1395–1413, https://doi.org/10.5194/tc-10-1395-2016, 2016.

Stigter, E. E., Steiner, J. F., Koch, I., Saloranta, T. M., Kirkham, J. D., and Immerzeel, W. W.: Energy and mass balance dynamics of the seasonal snowpack at two high-altitude sites in the Himalaya, Cold Regions Science and Technology, 183, 103 233, https://doi.org/10.1016/j.coldregions.2021.103233, 2021.

Stuefer, S. L., Kane, D. L., and Dean, K. M.: Snow Water Equivalent Measurements in Remote Arctic Alaska Watersheds, Water Resources Research, 56, 1–12, https://doi.org/10.1029/2019WR025621, 2020.

Tayleur, C. M., Devictor, V., Gaüzère, P., Jonzén, N., Smith, H. G., and Lindström, : Regional variation in climate change winners and losers highlights the rapid loss of cold-dwelling species, Diversity and Distributions, 22, 468–480, https://doi.org/10.1111/ddi.12412, 2016.

Thackeray, C. W., Derksen, C., Fletcher, C. G., and Hall, A.: Snow and Climate: Feedbacks, Drivers, and Indices of Change, Current Climate Change Reports, 5, 322–333, https://doi.org/10.1007/s40641-019-00143-w, 2019.

Tuzet, F., Dumont, M., Picard, G., Lamare, M., Voisin, D., Nabat, P., Lafaysse, M., Larue, F., Revuelto, J., and Arnaud, L.: Quantification of the radiative impact of light-absorbing particles during two contrasted snow seasons at Col du Lautaret (2058 m a.s.l., French Alps), Cryosphere, 14, 4553–4579, https://doi.org/10.5194/tc-14-4553-2020, 2020.

Tyler, N. J.: Climate, snow, ice, crashes, and declines in populations of reindeer and caribou (Rangifer tarandus L.), Ecological Monographs, 80, 197–219, https://doi.org/10.1890/09-1070.1, 2010.

Väliranta, M. and Mathijssen, P. J. H.: Geochemistry of Siikaneva peat core from Finland, https://doi.org/10.1594/PANGAEA.927689, 2021.

Varhola, A., Coops, N. C., Weiler, M., and Moore, R. D.: Forest canopy effects on snow accumulation and ablation: An integrative review of empirical results, Journal of Hydrology, 392, 219–233, https://doi.org/10.1016/j.jhydrol.2010.08.009, 2010.

Vernay, M., Lafaysse, M., Monteiro, D., Hagenmuller, P., Nheili, R., Samacoïts, R., Verfaillie, D., and Morin, S.: The S2M meteorological and snow cover reanalysis over the French mountainous areas: description and evaluation (1958-2021), Earth System Science Data, 14, 1707–1733, https://doi.org/10.5194/essd-14-1707-2022, 2022.

Verrelle, A., Glinton, M., Bazile, E., and P., L. M.: CERRA-Land : A new land surface reanalysis at 5.5 km resolution over Europe, in: EMS Annual Meeting Abstracts, vol. 18, p. 492, 2021.

Vionnet, V., Brun, E., Morin, S., Boone, A., Faroux, S., Le Moigne, P., Martin, E., and Willemet, J. M.: The detailed snowpack scheme Crocus and its implementation in SURFEX v7.2, Geoscientific Model Development, 5, 773–791, https://doi.org/10.5194/gmd-5-773-2012, 2012.

Voldoire, A., Sanchez-Gomez, E., Salas y Mélia, D., Decharme, B., Cassou, C., Sénési, S., Valcke, S., Beau, I., Alias, A., Chevallier, M., Déqué, M., Deshayes, J., Douville, H., Fernandez, E., Madec, G., Maisonnave, E., Moine, M. P., Planton, S., Saint-Martin, D., Szopa, S., Tyteca, S., Alkama, R., Belamari, S., Braun, A., Coquart, L., and Chauvin, F.: The CNRM-CM5.1 global climate model: Description and basic evaluation, Climate Dynamics, 40, 2091–2121, https://doi.org/10.1007/s00382-011-1259-y, 2013.

Voldoire, A., Saint-Martin, D., Sénési, S., Decharme, B., Alias, A., Chevallier, M., Colin, J., Guérémy, J. F., Michou, M., Moine, M. P., Nabat, P., Roehrig, R., Salas y Mélia, D., Séférian, R., Valcke, S., Beau, I., Belamari, S., Berthet, S., Cassou, C., Cattiaux, J., Deshayes, J., Douville, H., Ethé, C., Franchistéguy, L., Geoffroy, O., Lévy, C., Madec, G., Meurdesoif, Y., Msadek, R., Ribes, A., Sanchez-Gomez, E., Terray, L., and Waldman, R.: Evaluation of CMIP6 DECK Experiments With CNRM-CM6-1, Journal of Advances in Modeling Earth Systems, 11, 2177–2213, https://doi.org/10.1029/2019MS001683, 2019.

Webster, C. and Jonas, T.: Influence of canopy shading and snow coverage on effective albedo in a snow-dominated evergreen needleleaf forest, Remote Sensing of Environment, 214, 48–58, https://doi.org/10.1016/j.rse.2018.05.023, 2018.

Webster, C., Rutter, N., and Jonas, T.: Improving representation of canopy temperatures for modeling subcanopy incoming longwave radiation to the snow surface, Journal of Geophysical Research: Atmospheres, 122, 9154–9172, https://doi.org/10.1002/2017JD026581, 2017.

Westermann, S., Lüers, J., Langer, M., Piel, K., and Boike, J.: The annual surface energy budget of a high-arctic permafrost site on Svalbard, Norway, Cryosphere, 3, 245–263, https://doi.org/10.5194/tc-3-245-2009, 2009.